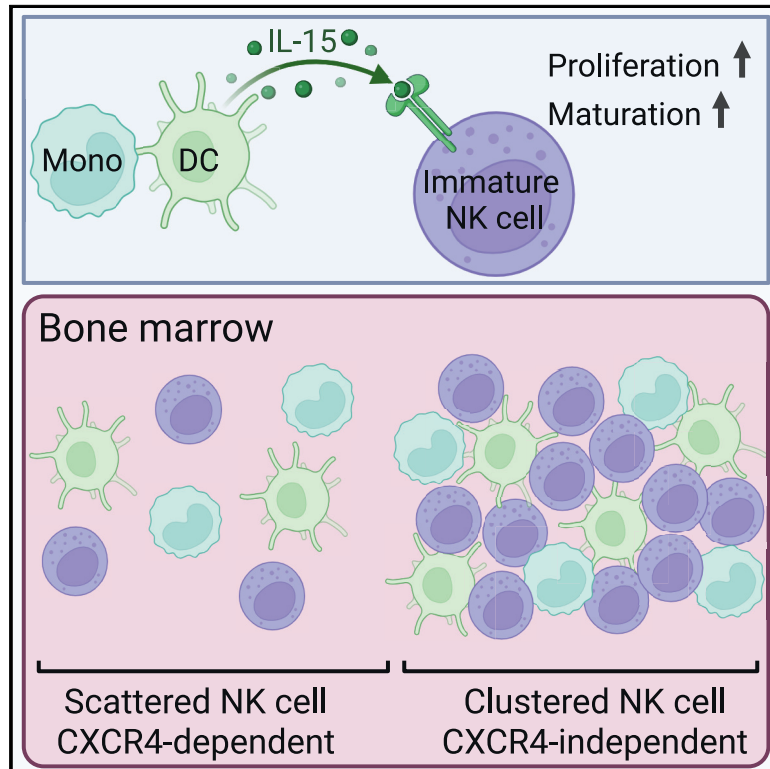# Hematopoietic cell-derived IL-15 supports NK cell development in scattered and clustered localization within the bone marrow

Graphical abstract

Highlights

- NK cell development in bone marrow depends on IL-15 produced by myeloid cells

- Developing NK cells are localized in bone marrow in scattered and clustered manners

- Scattered NK cells need CXCR4, while clustered NK cells overlap with myeloid cells

Authors

Shinya Abe, Takuma Asahi,
Takahiro Hara, ..., Veronika Sexl,
Takashi Nagasawa, Koichi Ikuta

Correspondence

ikuta.koichi.6c@kyoto-u.ac.jp

In brief

Abe et al. demonstrate the dependence of natural killer (NK) cell development on myeloid cell-derived interleukin-15 in the bone marrow. Using NK cell reporter mice, they identify scattered and clustered localization of NK cells. Scattered NK cells require CXCR4 expression, whereas clustered NK cells overlap with accumulations of myeloid cells.

Article

Hematopoietic cell-derived IL-15 supports NK cell development in scattered and clustered localization within the bone marrow

Shinya Abe,[1,2] Takuma Asahi,[1,2] Takahiro Hara,[1] Guangwei Cui,[1] Akihiro Shimba,[1,3] Shizue Tani-ichi,[1,3] Kohei Yamada,[1,4] Kazuko Miyazaki,[5] Hitoshi Miyachi,[6] Satsuki Kitano,[6] Naotoshi Nakamura,[7] Junichi Kikuta,[8] Alexis Vandenbon,[9] Masaki Miyazaki,[5] Ryo Yamada,[10] Toshiaki Ohteki,[11] Masaru Ishii,[8] Veronika Sexl,[12,14] Takashi Nagasawa,[13] and Koichi Ikuta[1,15,*]

[1]Laboratory of Immune Regulation, Department of Virus Research, Institute for Life and Medical Sciences, Kyoto University, Kyoto 606-8507, Japan
[2]Graduate School of Medicine, Kyoto University, Kyoto 606-8501, Japan
[3]Department of Human Health Sciences, Graduate School of Medicine, Kyoto University, Kyoto 606-8507, Japan
[4]Graduate School of Biostudies, Kyoto University, Kyoto 606-8501, Japan
[5]Laboratory of Immunology, Institute for Life and Medical Sciences, Kyoto University, Kyoto 606-8507, Japan
[6]Reproductive Engineering Team, Institute for Life and Medical Sciences, Kyoto University, Kyoto 606-8507, Japan
[7]Interdisciplinary Biology Laboratory (iBLab), Division of Natural Science, Graduate School of Science, Nagoya University, Nagoya 464-8602, Japan
[8]Department of Immunology and Cell Biology, Graduate School of Medicine and Frontier Biosciences, WPI Immunology Frontier Research Center, Osaka University, Suita 565-0871, Japan
[9]Laboratory of Tissue Homeostasis, Department of Biosystems Science, Institute for Life and Medical Sciences, Kyoto University, Kyoto 606-8507, Japan
[10]Statistical Genetics, Center for Genomic Medicine, Graduate School of Medicine, Kyoto University, Kyoto 606-8507, Japan
[11]Department of Biodefense Research, Medical Research Institute, Tokyo Medical and Dental University, Tokyo 113-8510, Japan
[12]Institute of Pharmacology and Toxicology, Department for Biomedical Sciences, University of Veterinary Medicine Vienna, 1210 Vienna, Austria
[13]Laboratory of Stem Cell Biology and Developmental Immunology, Graduate School of Frontier Biosciences and Graduate School of Medicine, WPI Immunology Frontier Research Center, Osaka University, Suita 565-0871, Japan
[14]Present address: University of Innsbruck, 6020 Innsbruck, Austria
[15]Lead contact
*Correspondence: ikuta.koichi.6c@kyoto-u.ac.jp
https://doi.org/10.1016/j.celrep.2023.113127

SUMMARY

Natural killer (NK) cells are innate immune cells critical for protective immune responses against infection and cancer. Although NK cells differentiate in the bone marrow (BM) in an interleukin-15 (IL-15)-dependent manner, the cellular source of IL-15 remains elusive. Using NK cell reporter mice, we show that NK cells are localized in the BM in scattered and clustered manners. NK cell clusters overlap with monocyte and dendritic cell accumulations, whereas scattered NK cells require CXCR4 signaling. Using cell-specific IL-15-deficient mice, we show that hematopoietic cells, but not stromal cells, support NK cell development in the BM through IL-15. In particular, IL-15 produced by monocytes and dendritic cells appears to contribute to NK cell development. These results demonstrate that hematopoietic cells are the IL-15 niche for NK cell development in the BM and that BM NK cells are present in scattered and clustered compartments by different mechanisms, suggesting their distinct functions in the immune response.

INTRODUCTION

Natural killer (NK) cells are innate immune cells critical for responses to infection and tumor.[1,2] NK cells develop in the bone marrow (BM) in an interleukin-15 (IL-15)-dependent manner and eliminate target cells by direct cytotoxicity and interferon-γ (IFN-γ). Recently, NK cells have been recategorized as innate lymphoid cells (ILCs). Group 1 ILCs include conventional NK cells and type 1 ILCs (ILC1s) and express the transcription factor (TF) T-bet and IFN-γ.[2–4] In contrast, the TF Eomes is expressed in NK cells but not in ILC1s, distinguishing these two subsets in the mouse.[5–7] Both NK cells and ILC1s differentiate from common lymphoid progenitors (CLPs), but then develop through a distinct lineage via different progenitors in the BM.[8–11] The earliest stage of NK cell development is pre-NK progenitors (pre-NKPs). Pre-NKPs then differentiate into refined NKPs (rNKPs), which further differentiate into immature NK (iNK) cells and then mature NK (mNK) cells. In addition, many TFs, such as STAT5, Tbx21, Nfil3, and Id2, are involved in the development and maturation of NK cells and ILC1s.[11,12]
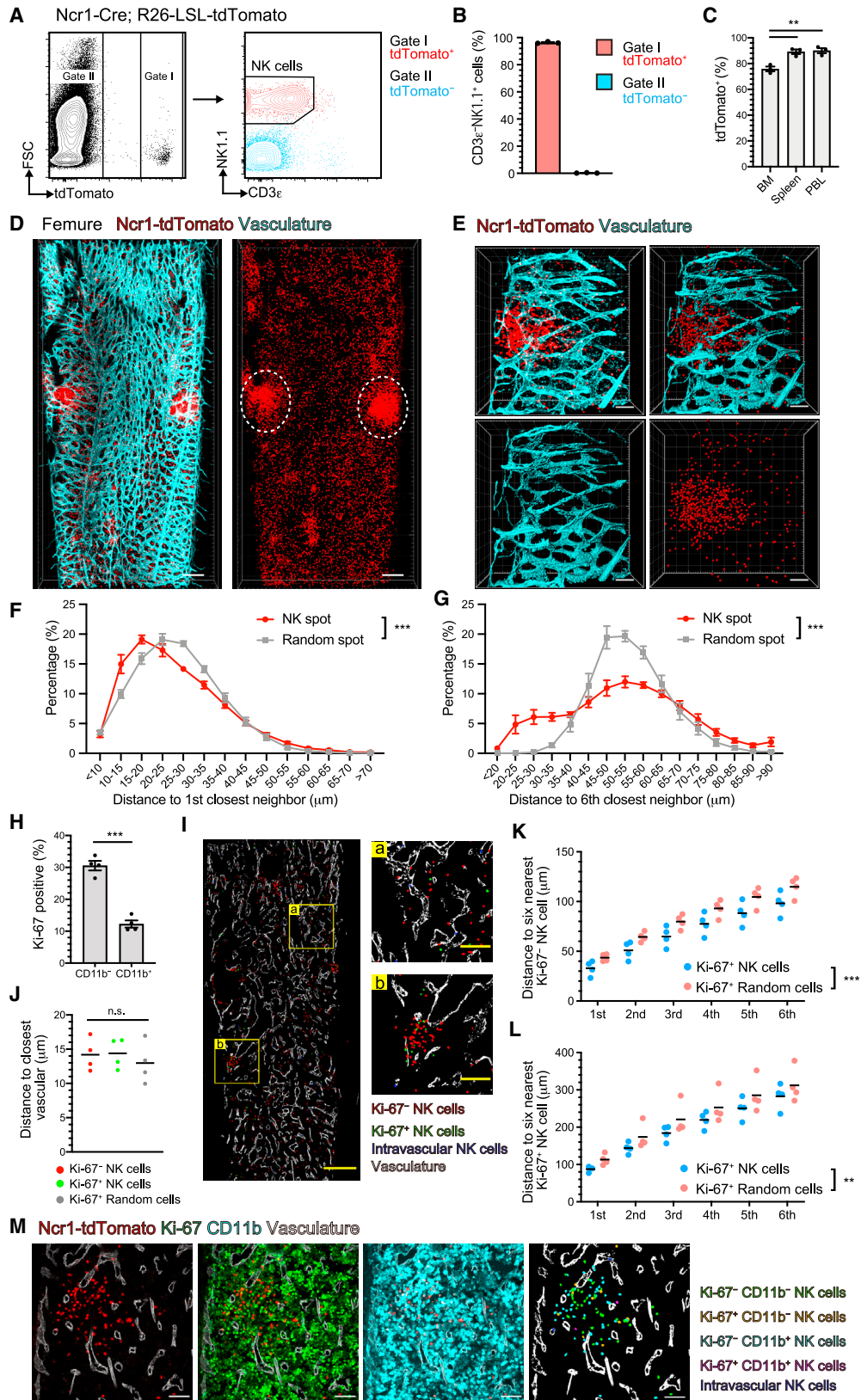
(legend on next page)

IL-15 is a cytokine critical for the development and homeostasis of natural killer T (NKT) cells, memory CD8 T cells, intraepithelial lymphocytes (IELs), and group 1 ILCs.[5,8,13,14] IL-15 forms a complex with the IL-15 receptor α (IL-15Rα), which is trans-presented to target cells and activates STAT5 and phosphatidylinositol 3-kinase (PI3K).[15–17] To date, many sources of IL-15 have been identified using cell-specific IL-15- or IL-15Rα-deficient mice. Hepatocytes, intestinal epithelial cells, adipocytes, and thymic epithelial cells have been identified as IL-15 sources essential for IL-15-dependent cells such as NK cells.[18–22] In addition, IL-15 produced by dendritic cells (DCs) and macrophages is critical for maintaining NK cells and memory CD8 T cells in secondary lymphoid organs.[18,21] Although the BM is the major site of NK cell development, the cellular source of IL-15 essential for NK cell development is unknown.

BM niches are specialized microenvironments composed of mesenchymal stromal cells, blood vascular endothelial cells, and differentiated hematopoietic cells that regulate the maintenance and differentiation of hematopoietic stem cells (HSCs) and progenitor cells.[23] CXCL12-abundant reticular (CAR) cells that overlap with leptin receptor⁺ (Lepr⁺) stromal cells express the stem cell factor (SCF), CXCL12, and IL-7, which are essential for HSC homeostasis and B lymphopoiesis.[24–28] As for NK cells, natural cytotoxicity triggering receptor 1 (Ncr1, also known as NKp46)-expressing bulk NK cells are localized adjacent to CAR cells,[29] and NK cell development is severely diminished in Mx1-Cre-, Flt3-Cre-, and IL-7Rα-Cre-specific CXCR4 (the receptor for CXCL12)-deficient mice.[25,29] Previously, we identified PDGFRβ⁺ stromal cells as prominent IL-15-producing stromal cells in the BM using IL-15 reporter mice.[30] Some CAR cells are reported to express both IL-15 and IL-15Rα, suggesting that IL-15 produced by CAR cells may be involved in NK cell development.[29] On the other hand, hematopoietic progenitors and myeloid cells in the BM have been reported to express IL-15 in other IL-15 reporter mice.[31] Therefore, it remains unclear whether IL-15 produced by CAR cells or other types of BM cells is essential for NK cell development in the BM.

To investigate the cellular niche for NK cells, we analyzed the distribution of developing NK cells in the BM. NK cells were distributed in scattered and clustered manners. Scattered NK cells depended on their CXCR4 expression, whereas clustered NK cells overlapped with accumulations of CX3CR1⁺ myeloid cells. Furthermore, developing NK cells in the BM were severely reduced in hematopoietic cell-specific, but not stromal cell-specific, IL-15-deficient mice. This study identifies two types of developing NK cells in the BM with distinct localization and CXCL12 dependence and demonstrates that hematopoietic cell-derived IL-15 is essential for NK cell development in the BM.

RESULTS

Developing NK cells are present in scattered and clustered manners in the BM

To investigate the distribution of developing NK cells in the BM, we analyzed Ncr1-iCre;Rosa26-LSL-tdTomato (hereafter referred to as Ncr1-tdTomato) mice by flow cytometry (FCM). More than 95% of the tdTomato⁺ cells were CD3ε⁻NK1.1⁺ cells, most of which were NK cells (Figures 1A and 1B). Approximately 70% of the CD3ε⁻NK1.1⁺ cells expressed tdTomato in the BM (Figure 1C). Because the frequency of tdTomato⁺ cells was slightly higher in CD11b⁺ mature NK cell fractions than in CD11b⁻ immature NK cell fractions (Figure S1A), the percentage of tdTomato⁺ within the CD3ε⁻NK1.1⁺ cells was lower in the BM than in the spleen and peripheral blood (PB) (Figure 1C). Combined with the CUBIC tissue-clearing technique,[32] we obtained deep three-dimensional (3D) images of Ncr1-tdTomato⁺ cells in the BM and spleen. Consistent with the previous study,[33] Ncr1-tdTomato⁺ cells were mainly distributed in the sinusoidal vascular-rich red pulp region of the spleen (Figure S1B), confirming that the combination of the reporter mice and tissue-clearing method correctly identified the localization of NK cells in organs. Interestingly, Ncr1-tdTomato⁺ cells were distributed in the BM of the femur in two ways, one evenly scattered and the other occasionally forming distinct clusters (Figures 1D and S1C). The NK cell clusters

Figure 1. Some NK cells cluster in the BM

(A and B) Representative FCM plots of BM cells (A) and frequency of NK cells (CD3ε⁻NK1.1⁺) in gates I and II (B) from Ncr1-Cre⁺;Rosa26^tdTomato/⁺ (Ncr1-tdTomato) mice (n = 3).

(C) Frequency of tdTomato⁺ cells among NK cells in the BM, spleen, and PB (n = 3).

(D and E) Representative confocal images of a large field with 200-μm-thick (D) and clustered regions with 150-μm-thick (E) tissue-cleared femur specimens from Ncr1-tdTomato mice. Red, Ncr1-tdTomato; cyan, VE-cadherin⁺ and CD31⁺ blood vessels. White dotted circles indicate clustered NK cell regions (D). Scale bars, 300 μm (D) and 70 μm (E).

(F and G) Percentage of NK cells with indicated distances to the nearest NK cell (F) and the sixth nearest NK cell in 3D reconstructed confocal images of tissue-cleared femur specimens (G) (n = 8).

(H) Frequency of Ki-67⁺ cells within the CD11b⁻ immature or CD11b⁺ mature NK cell fractions in the BM of WT mice (n = 4).

(I) Representative images of *in situ* mapping of NK cell subsets in the BM. Ncr1-tdTomato⁺ NK cells were divided into three subsets defined by the Ki-67 expression and intravascular localization. Red, parenchymal Ki-67⁻ NK cells; green, parenchymal Ki-67⁺ NK cells; blue, intravascular NK cells; white, vasculature. (a) Scattered NK cell region. (b) Clustered NK cell region. Scale bars, 300 μm (left) and 100 μm (right).

(J–L) Mean distance of each Ki-67⁺ NK, Ki-67⁻ NK, or Ki-67⁺ random cell to the nearest vasculature (J). Histograms show the average distance of each Ki-67⁺ NK cell and Ki-67⁺ random cell to the sixth nearest Ki-67⁻ NK cell (K) or Ki-67⁺ NK cell (L). A total of 273 Ki-67⁺ NK cells, 273 Ki-67⁺ random cells, and 1,927 Ki-67⁻ NK cells from four tibia sections were analyzed (n = 4 independent experiments).

(M) The first three panels from the left show confocal images of the tibia from Ncr1-tdTomato mice. Red, Ncr1-tdTomato; green, Ki-67; cyan, CD11b; white, vasculature. The right panel shows *in situ* mapping of subdivided NK cells based on the Ki-67 and CD11b expression. Green, Ki-67⁻CD11b⁻ NK cells; cyan, Ki-67⁻CD11b⁺ NK cells; orange, Ki-67⁺ CD11b⁻ NK cells; magenta, Ki-67⁺CD11b⁺ NK cells; blue, intravascular NK cells. Scale bars, 50 μm.

Data are mean ± SEM with non-statistical analysis (B), unpaired two-tailed Student's t test (H), one-way ANOVA and Tukey's multiple comparison test (C) or two-way ANOVA (F and G), mean with one-way ANOVA (J) or two-way ANOVA (K and L), and pooled from 3–4 independent experiments. **p < 0.01; ***p < 0.001. Data represent at least three independent experiments with similar results (A, D, E, I, and M). See also Figure S1.
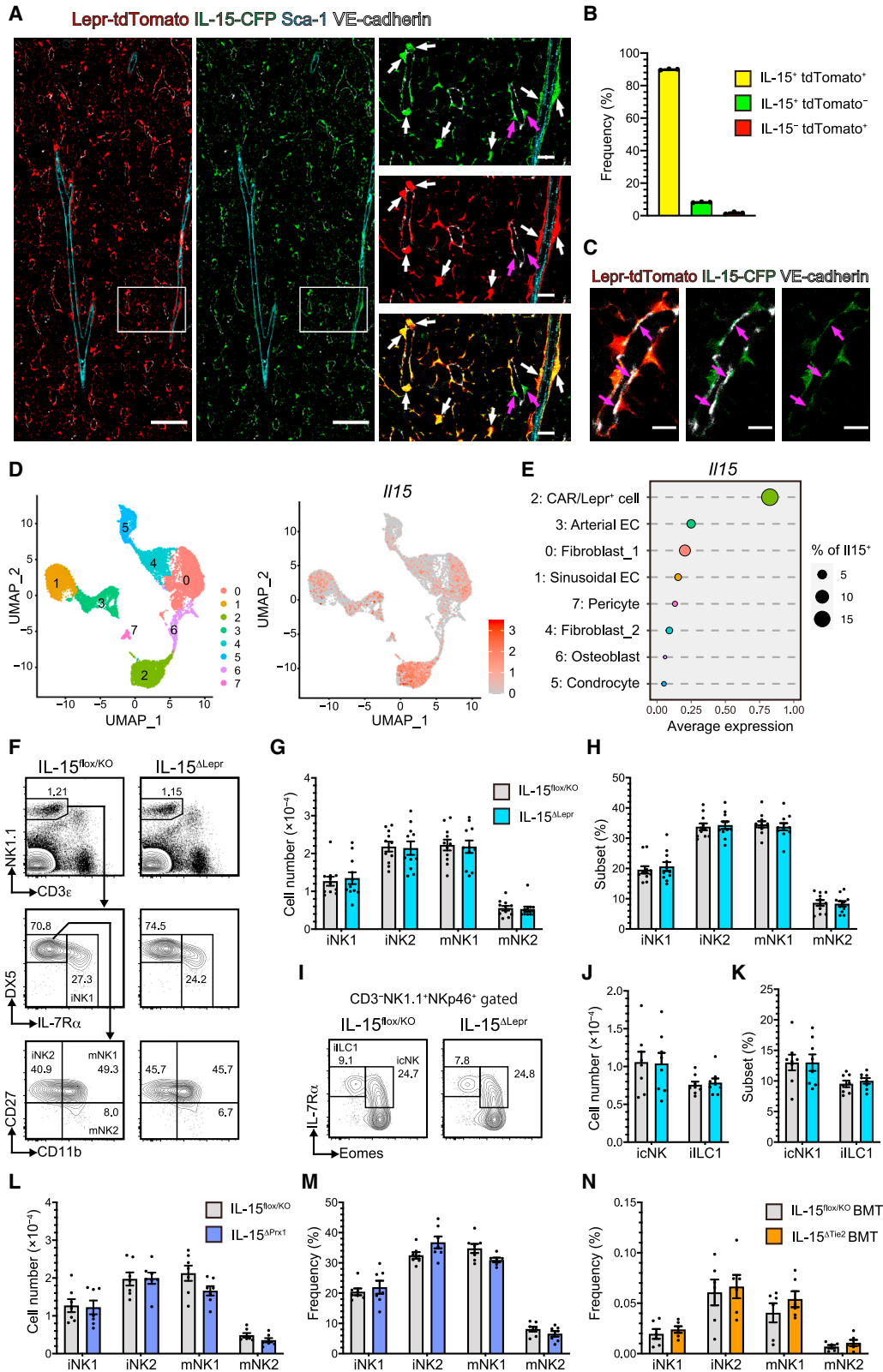
(legend on next page)

spanned the vascular network of the BM parenchyma (Figure 1E). Immunohistochemistry with anti-Ncr1 antibody also confirmed this unique NK cell distribution (Figure S1D). We also observed NK cell clusters in other bones, including the tibia, ilium, and sternum (Figure S1E). We compared the relationship between the 3D reconstructed NK cell positions. The distance of arbitrary NK cells to the nearest NK cells was shorter than that of randomly placed cells (Figure 1F). Notably, the distribution of distances to the sixth nearest NK cell indicates that some NK cells are in close proximity (<30 μm), whereas randomly placed cells had a symmetric and uniform distribution (Figure 1G). These data indicate that some NK cells are located close to each other and form clusters.

To test whether NK cell development is associated with oneof the two distributions in the BM, we analyzed the expression of Ki-67, a cell-proliferation marker, in NK cells. Ki-67$^+$ NK cells were enriched in the immature CD11b$^-$ NK cell population (Figure 1H). We evaluated the distribution of proliferating immature NK cells within the BM. Ncr1-tdTomato$^+$ NK cells were classified into intravascular NK cells, Ki-67$^+$ parenchymal NK cells, and Ki-67$^-$ parenchymal NK cells. Ki-67$^+$ NK cells were present in clustered and scattered regions (Figure 1I). We next examined the relationship between the NK cell subpopulations and blood vessels. The distance of Ki-67$^+$ NK cells to the nearest blood vessel was similar to that of Ki-67$^+$ random cells and Ki-67$^-$ NK cells (Figure 1J), suggesting that NK cell development is not dependent on the vascular niche. Next, we analyzed the distance between NK cells. The distance of each Ki-67$^+$ NK cell to the nearest Ki-67$^-$ NK cell or Ki-67$^+$ NK cell was significantly closer than that of Ki-67$^+$ random cells (Figures 1K and 1L). In contrast, the distance of each Ki-67$^+$ NK cell to the nearest intravascular NK cell was similar to that of each Ki-67$^+$ random cell (Figure S1F). These results suggest that Ki-67$^+$ proliferating NK cells tend to localize near both Ki-67$^+$ and Ki-67$^-$ NK cells. Furthermore, *in situ* mapping showed that NK cell clusters contained CD11b$^-$ immature and CD11b$^+$ mature NK cells (Figure 1M). The frequency of Ki-67$^+$ proliferating NK cells and CD11b$^+$ mature NK cells remained unchanged between clustered and scattered regions, whereas intravascular NK cells were less proliferative and more enriched in mature NK cells than parenchymal NK cells (Figures S1G and S1H). These data suggest that the NK cluster contains proliferating immature NK cells, similar to the scattered region.

NK cell development in the BM does not depend on stromal cell-derived IL-15

Although IL-15 is required for the development and maintenance of NK cells, the cellular source of IL-15 essential for NK cell development in the BM is uncertain. To confirm the identity of IL-15-producing stromal cells, we analyzed Lepr-Cre;R26-LSL-tdTomato;IL-15-CFP double-reporter mice. IL-15/CFP was highly expressed in Lepr-tdTomato$^+$ stromal cells, which were composed of both blood-vessel-surrounding and -non-surrounding types (Figure 2A). More than 90% of IL-15$^+$ cells and tdTomato$^+$ cells overlapped, but a small population also expressed IL-15 but not tdTomato (less than 10%) (Figure 2B). Furthermore, no IL-15/CFP signal was detected in sinusoidal endothelial cells, osteoblasts, and adipocytes (Figures 2C, S2A, and S2B). Consistently, reanalysis of the single-cell RNA sequencing (scRNA-seq) data shows that CAR/Lepr$^+$ mesenchymal stromal cells expressed IL-15 more strongly than other stromal cells (Figures 2D, 2E, and S2C).[34] Taken together, CAR/Lepr$^+$ stromal cells are a predominant population expressing IL-15 in the BM.

To investigate whether IL-15 derived from CAR/Lepr$^+$ stromal cells is essential for NK cell development, we analyzed CAR/Lepr$^+$ cell-specific Lepr-Cre;IL-15-flox (IL-15$^{\Delta Lepr}$) mice. Here, IL-15 mRNA was drastically reduced in CAR/Lepr$^+$ cells (Figure S2D). To analyze NK cells by FCM, we classified CD3ε$^-$NK1.1$^+$ NK cells into four developmental stages based on the expression of DX5, IL-7 receptor α (IL-7Rα), CD27, and CD11b: IL-7Rα$^+$ immature NK1 (iNK1), IL-7Rα$^-$DX5$^+$CD27$^+$CD11b$^-$ immature NK2 (iNK2), IL-7Rα$^-$DX5$^+$CD27$^+$CD11b$^+$ mature NK1 (mNK1), and IL-7Rα$^-$DX5$^+$CD27$^-$CD11b$^+$ mature NK2 (mNK2) cells, with a developmental sequence of iNK1, iNK2, mNK1, and mNK2 (Figure S2E). We further subdivided the iNK1 fraction into Eomes$^+$ immature conventional NK cells (icNK) and Eomes$^-$ immature ILC1s (iILC1s) (Figure S2F). Unexpectedly, the number and frequency of NK cells and ILC1s were unchanged at each stage in the BM, spleen, and PB of IL-15$^{\Delta Lepr}$ mice (Figures 2F–2K, S2G, and S2H). We also examined Prx1-Cre;IL-15-flox (IL-15$^{\Delta Prx1}$) mice, in which IL-15 is deleted in all mesenchymal cells, including osteoblasts, chondrocytes, and CAR/Lepr$^+$ stromal cells. Consistent with the results of the IL-15$^{\Delta Lepr}$ mice, there was no difference in the BM NK cells from IL-15$^{\Delta Prx1}$ mice (Figures 2L and 2M). Next, we investigated the contribution of IL-15 derived from blood vascular endothelial

---

Figure 2. NK cell development in the BM is not dependent on stromal cell-derived IL-15

(A) Representative confocal images of the femur from Lepr-Cre$^+$;Rosa26$^{tdTomato/+}$;IL-15$^{CFP/+}$ mice. The right column shows higher magnification of the solid white squares and Lepr-tdTomato$^+$IL-15-CFP$^+$ stromal cells (white arrows) and Lepr-tdTomato$^-$IL-15-CFP$^+$ stromal cells (magenta arrows). Red, Lepr-tdTomato; green, IL-15-CFP; cyan, Sca-1; white, VE-cadherin. Scale bars, 300 μm (left and middle) and 50 μm (right).

(B) Frequency of the indicated stromal cell populations in the femur (n = 3).

(C) Representative confocal images show IL-15-CFP$^-$VE-cadherin$^+$ sinusoidal endothelial cells (magenta arrows). Scale bars, 10 μm.

(D and E) scRNA-seq data of BM stromal cells (GSE128423) underwent a uniform manifold approximation and projection (UMAP) analysis (D). The average expression of *Il15* in each cell population assigned in Figure S2C is shown (E).

(F–H) Representative FCM plots (F), absolute number (G), and frequency (H) of NK cells at each developmental stage in the BM from Lepr-Cre$^+$;IL-15$^{flox/KO}$ (IL-15$^{\Delta Lepr}$) and IL-15$^{flox/KO}$ mice (n = 11).

(I–K) Representative FCM plots (I), absolute number (J), and frequency (K) of IL-7Rα$^+$ immature NK cell populations in BM from IL-15$^{\Delta Lepr}$ and IL-15$^{flox/KO}$ mice (n = 8).

(L and M) Absolute number (L) and frequency (M) of NK cells at each developmental stage from Prx1-Cre$^+$;IL-15$^{flox/KO}$ (IL-15$^{\Delta Prx1}$) and IL-15$^{flox/KO}$ mice (n = 7).

(N) Frequency of NK cells at each developmental stage from Tie2-Cre$^+$;IL-15$^{flox/KO}$ (IL-15$^{\Delta Tie2}$) and IL-15$^{flox/KO}$ mice after transplantation of BM cells from WT mice (n = 6).

Data are mean ± SEM with non-statistical analysis (B) and unpaired two-tailed Student's t test (G, H, J, K, L, M, and N) pooled from 3–8 independent experiments. Data represent at least three independent experiments with similar results (A, C, F, and I). See also Figure S2.

A Ncr1-Cre; R26-LSL-tdTomato
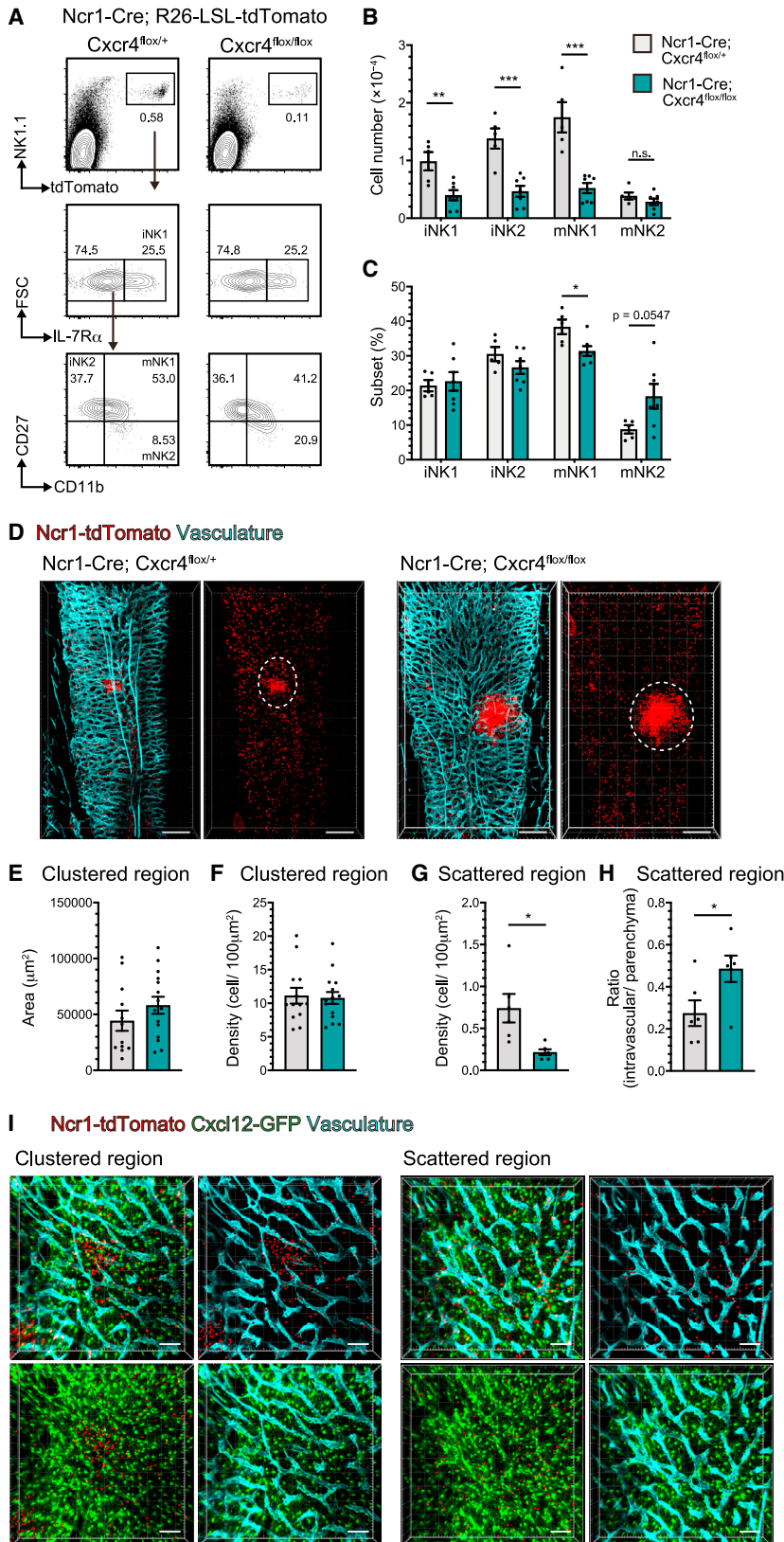
Figure 3. CXCR4 is required for NK cell retention in the BM

(A) Representative FCM plots of NK cells in the BM from Ncr1-Cre+;Rosa26tdTomato/+;Cxcr4flox/flox and Ncr1-Cre+;Rosa26tdTomato/+;Cxcr4flox/+ mice. tdTomato+ NK cells were further subdivided into each developmental stage.

(B and C) Absolute number (B) and frequency (C) of tdTomato+ NK cells at each developmental stage in the BM, as shown in (A) (n = 5–7).

(D) Representative confocal images of 200-μm-thick femur specimens from Ncr1-Cre+;Rosa26tdTomato/+; Cxcr4flox/flox and Ncr1-Cre+;Rosa26tdTomato/+;Cxcr4flox/+ mice. Red, Ncr1-tdTomato; cyan, VE-cadherin+ and CD31+ blood vessels. White dotted circles indicate clustered NK cell regions. Scale bars, 300 μm.

(E and F) Area (E) and NK cell density (F) of clustered regions shown in (D). Each data point in the bar graphs represents a single clustered region (n = 7).

(G and H) NK cell density (G) and ratio of intravascular to parenchymal NK cells (H) in scattered regions from the confocal image of a thin specimen (n = 6–7). NK cell cluster regions were excluded from the analysis.

(I) Representative confocal images of 70-μm-thick clustered and scattered NK cell area from Ncr1-Cre+;Rosa26tdTomato/+;CXCL12GFP/+ mice. Red, Ncr1-tdTomato; green, CXCL12-GFP; cyan, vasculature. Scale bars, 50 μm.

Data are mean ± SEM with unpaired two-tailed Student's t test (B, C, E, F, G, and H). Data were pooled from six independent experiments (B and C). *p < 0.05; **p < 0.01; ***p < 0.001; n.s., not significant. Data represent at least three independent experiments with similar results (D and E). See also Figure S3.

cells (BECs). We transplanted wild-type (WT) BM cells into Tie2-Cre;IL15-flox (IL-15$^{\Delta Tie2}$) mice because Tie2-Cre was expressed in both BECs and HSCs. The frequency of the NK cell subpopulations was unchanged in the BM 5 weeks after the transplantation (Figure 2N). We also examined memory-phenotype CD8 T and NKT cells in the BM (Figure S2I). The number and frequency of CD44$^+$ memory-phenotype CD8 T cells, CD1d-tetramer (CD1d-tet)$^+$ invariant NKT (iNKT) cells, and CD1d-tet$^-$ variant NKT (vNKT) cells were unchanged in IL-15$^{\Delta Lepr}$ mice (Figures S2J and S2K). Taken together, IL-15 produced by BM stromal cells is not required for NK cell development in the BM.

The CXCL12/CXCR4 axis is required for scattered NK cells in the BM

Although BM stromal cell-derived IL-15 was dispensable for NK cell development, it remains unknown whether BM stromal cells contribute to NK cell development by other mechanisms. The CXCL12/CXCR4 axis is one of the mechanisms by which BM stromal cells attract and retain HSCs in the BM.[35,36] During NK cell differentiation, CXCR4 expression is high at the immature stage and decreases with maturation.[37–39] Consistently, CXCR4 expression was gradually reduced from the iNK1 to the mNK1 stage (Figures S3A and S3B). To determine the role of CXCR4 after NK cell commitment, we crossed Ncr1-iCre;Cxcr4-flox (Cxcr4$^{\Delta Ncr1}$) mice with Rosa26-LSL-tdTomato mice. Except for mNK2 in Cxcr4$^{\Delta Ncr1}$ mice, NK cell subsets were significantly reduced to less than half that of control mice (Figures 3A–3C). Consistent with the previous report,[37] most of the intravascular NK cells were mNK2 cells, similar to PB in WT mice (Figures S3C–S3E). Thus, the number of mNK2 cells may not be affected by CXCR4 ablation. In contrast, the reduction in NK cell numbers in the spleen and PB caused by CXCR4 ablation was small compared to that in the BM (Figures S3F–S3I). This result suggests that the impaired NK cell development in the BM caused by CXCR4 deficiency was partially restored in the peripheral tissues.

Next, we analyzed the distribution of NK cells in the BM of Cxcr4$^{\Delta Ncr1}$ mice. Surprisingly, NK cell clusters were present in this BM, whereas scattered NK cells were reduced (Figure 3D). The area and NK cell density of clustered regions were unchanged in CXCR4$^{\Delta Ncr1}$ mice (Figures 3E and 3F). In contrast, parenchymal NK cells in scattered regions were significantly reduced in CXCR4$^{\Delta Ncr1}$ mice, and the ratio of intravascular to parenchymal NK cells was increased (Figures 3G and 3H). These results suggest that CXCR4 contributes to the retention or trafficking of NK cells in the scattered region. Next, we tested whether CAR/Lepr$^+$ stromal cells associate with NK cell clusters in the BM using Ncr1-tdTomato;Cxcl12-GFP double-reporter mice. CAR cells were uniformly distributed in the BM without specific co-localization with the NK cell clusters (Figure 3I). Similar results were obtained with Ncr1-tdTomato;IL-15-CFP double-reporter mice (Figure S3J). These results suggest that BM stromal cells maintain scattered NK cells in the BM but do not contribute to IL-15-mediated NK cell development.

IL-15 produced by hematopoietic cells is essential for NK cell development in the BM

To test whether hematopoietic cell-derived IL-15 plays a role in NK cell development, we analyzed hematopoietic cell-specific

IL-15 conditional knockout (cKO) (Vav-Cre;IL-15-flox, IL-15$^{\Delta Vav}$) mice. The Vav-Cre transgene efficiently targeted hematopoietic cells but not stromal cells in the BM (Figure S4A). In IL-15$^{\Delta Vav}$ mice, the number of NK cells was severely reduced at all stages of development (Figures 4A and 4B). Because the reduction of mature NK cells was more pronounced than that of immature NK cells, the frequency of iNK1 cells among NK cells was relatively high (Figure 4C). This observation was further supported by a comparable analysis of systemic IL-15 KO mice (Figures S4B and S4C). In addition, the numbers of both icNK cells and iILC1s were reduced in IL-15$^{\Delta Vav}$ mice, whereas their frequencies were increased in NK cells (Figures 4D–4F). Consistent with IL-15$^{\Delta Vav}$ mice, the number of BM NK cells was significantly decreased in IL-15$^{\Delta Tie2}$ mice before BM transplantation (Figures S4D and S4E). In contrast, rNKP and ILC progenitor cell numbers were unchanged in IL-15$^{\Delta Vav}$ mice (Figures 4G–4I, S4F, and S4G). These data are consistent with those obtained in IL-15 KO mice (Figure 4J). These results suggest that hematopoietic cell-derived IL-15 is essential for the development of early NK cells and ILC1s in the BM.

IL-15 mRNA levels in the whole BM showed that IL-15 mRNA was almost absent in IL-15$^{\Delta Vav}$ mice but not in IL-15$^{\Delta Lepr}$ mice (Figures 4K and 4L). Thus, the major source of IL-15 in the BM appears to be hematopoietic cells, with a limited contribution from stromal cells. In addition to NK cells, the number and frequency of CD44$^+$ memory-phenotype CD8 T cells and CD1d-tet$^-$ variant NKT (vNKT) cells were significantly reduced in the BM of IL-15$^{\Delta Vav}$ mice (Figures S4H–S4J). These results suggest that hematopoietic cell-derived IL-15 is required for memory-phenotype CD8 T and vNKT cells in the BM.

IL-15 produced by monocytes and dendritic cells partially contributes to NK cell development in the BM

Next, we investigated which hematopoietic cells produce IL-15 essential for NK cell development in the BM. Reanalysis of published scRNA-seq data from BM showed that different types of hematopoietic cells, including c-kit$^+$ progenitors, neutrophils, and monocytes, expressed IL-15 (Figures 5A, 5B, and S5A).[40] To examine the effect of IL-15 produced by distinct hematopoietic cells in the BM, we analyzed LysM- or CD11c-Cre;IL-15-flox (IL-15$^{\Delta LysM}$ and IL-15$^{\Delta CD11c}$) mice. We confirmed the specificity and efficiency of LysM-Cre and CD11c-Cre mice by crossing them with Rosa26-LSL-tdTomato mice. While tdTomato was detected in many immune cells in both mice, CD11c-Cre- and LysM-Cre-mediated recombination was efficient in DCs and neutrophils, respectively (Figures S5B and S5C). IL-15$^{\Delta LysM}$ and IL-15$^{\Delta CD11c}$ mice showed significantly reduced mNK1 and mNK2 cells in the BM, which was milder than in IL-15$^{\Delta Vav}$ mice (Figures 5C–5F). Furthermore, LysM-Cre and CD11c-Cre double cKO mice had synergistically fewer NK cells than single cKO mice, which was still milder than Vav-Cre cKO mice (Figures S5D and S5E). These data suggest that neutrophils, monocytes, DCs, and other hematopoietic cells produce IL-15 important for NK cell development. To test which type of hematopoietic cell supports NK cells, we co-cultured NK cells with these hematopoietic cells. NK cells were better maintained in co-culture with WT monocytes than with IL-15-deficient monocytes or without monocytes (Figures 5G and 5H). In contrast, co-cultures
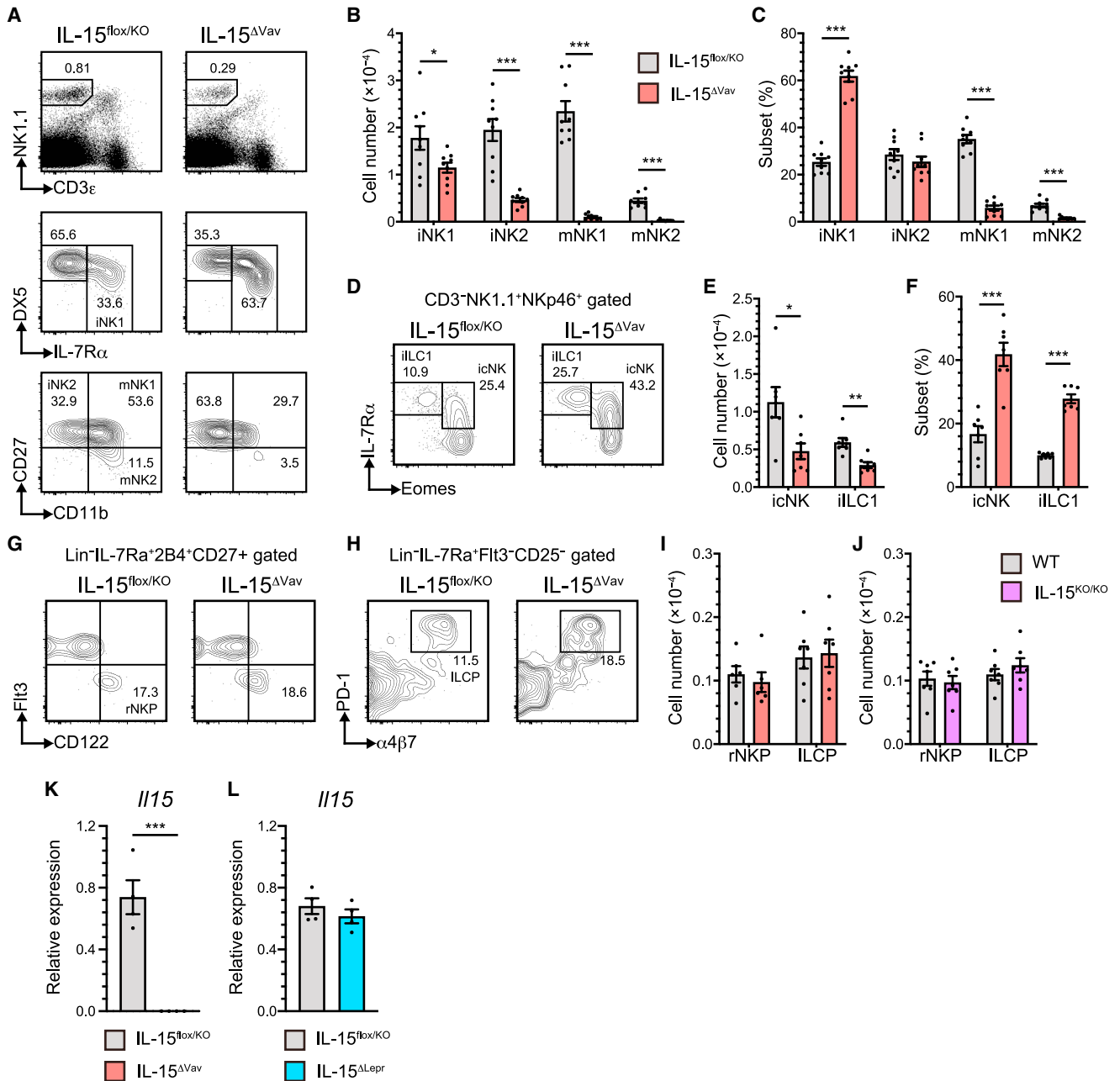
Figure 4. Hematopoietic cell-derived IL-15 is essential for NK cell development in the BM

(A–C) Representative FCM plots (A), absolute number (B), and frequency (C) of NK cells at each developmental stage in the BM from Vav-Cre[+];IL-15[flox/KO] (IL-15[ΔVav]) and IL-15[flox/KO] mice (n = 9).

(D–F) Representative FCM plots (D), absolute number (E), and frequency (F) of the IL-7Rα[+] immature NK cell population in the BM from IL-15[ΔVav] and IL-15[flox/KO] mice (n = 7).

(G and H) Representative FCM plots of rNKP (Lin^{−}IL-7Rα^{+}CD27^{+}2B4^{+}Flt3^{−}IL-2Rβ^{+}) (G) and ILC progenitor (ILCP) (Lin^{−}Flt3^{−}CD25^{−}α4β7^{+}PD-1^{+}) (H) cells in the BM from IL-15[ΔVav] and IL-15[flox/KO] mice.

(I and J) Absolute numbers of rNKP and ILCP cells in the BM from IL-15[ΔVav] and IL-15[flox/KO] mice (I) (n = 6–7) and IL-15[KO/KO] and WT mice (J) (n = 7).

(K and L) *Il15* mRNA expression in the whole BM from IL-15[ΔVav] and IL-15[flox/KO] mice (K) and IL-15[ΔLepr] and IL-15[flox/KO] mice (L) (n = 4). Expression levels were normalized to *Hprt*.

Data are mean ± SEM with unpaired two-tailed Student's t test (B, C, E, F, I, J, K, and L) and pooled from 4–7 independent experiments. *p < 0.05; **p < 0.01; ***p < 0.001. Data represent at least five independent experiments with similar results (A, D, G, and H). See also Figure S4.

I Ncr1-tdTomato CX3CR1-GFP Vasculature DAPI

J Ncr1-tdTomato CX3CR1-GFP I-A/I-E
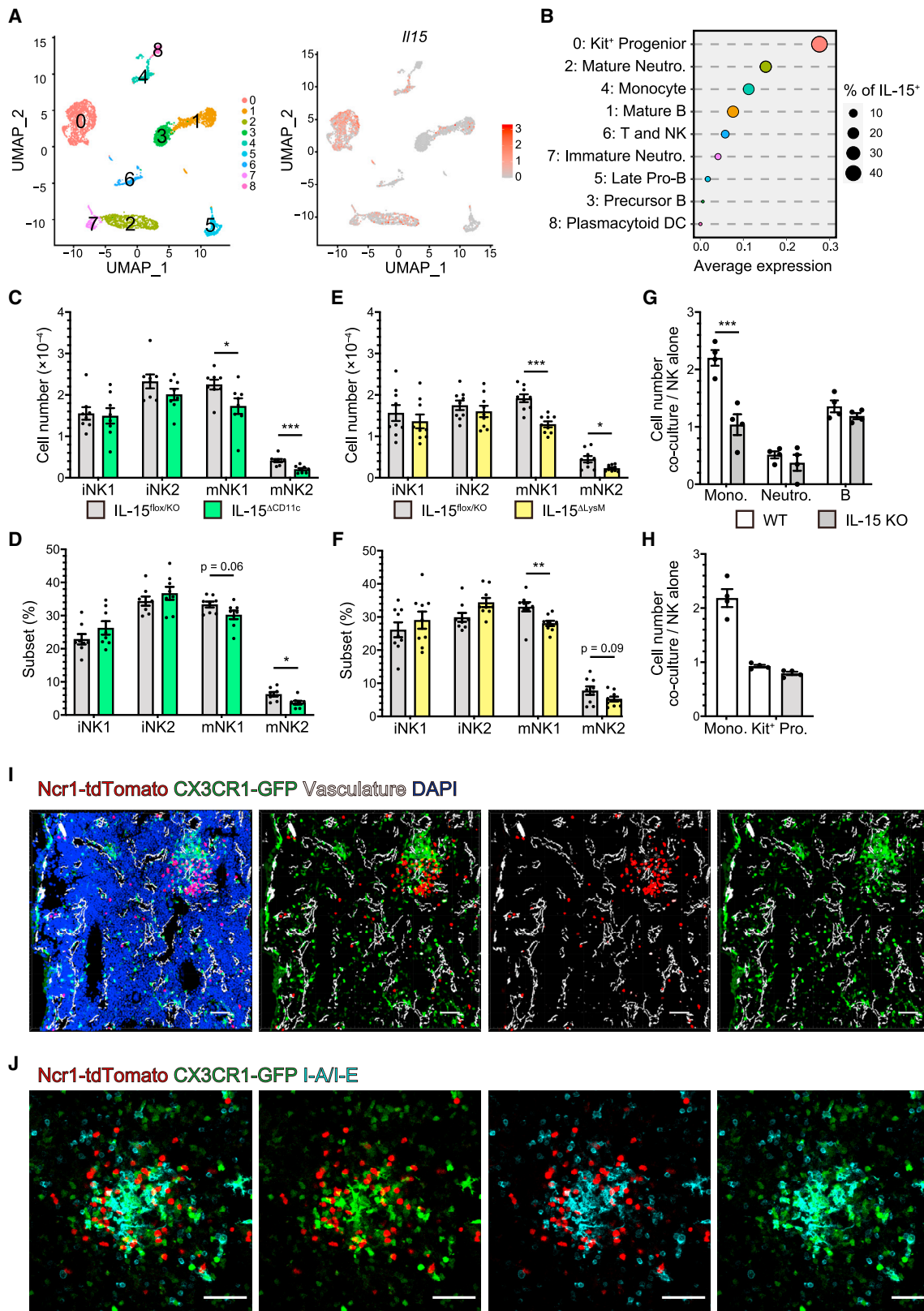
(legend on next page)

with neutrophils, B cells, and c-kit[+] hematopoietic progenitors did not maintain NK cells. These results suggest that monocytes may produce IL-15 important for NK cell development in the BM.

Next, we used CX3CR1-GFP mice to examine the co-localization of NK and myeloid cells. A bright GFP signal was detected in BM monocytes and DCs. In Ncr1-tdTomato;CX3CR1-GFP double-reporter mice, we found NK cell clusters associated with CX3CR1-GFP[+] cell clusters that included I-A/I-E[+] reticular DCs and GFP[bright] ring-shaped monocytes (Figures 5I and 5J). These results suggest that some NK cells in the BM form clusters with CX3CR1-GFP^{+} myeloid cells, which may allow efficient transmission of the IL-15 signaling.

In addition to NK cells, the number and frequency of CD44^{+} memory-phenotype CD8 T cells were significantly reduced in the BM of IL-15[ΔCD11c] mice but not in IL-15[ΔLysM] mice (Figures S5F and S5G), whereas the number of CD1d-tet^{−} vNKT cells was reduced in IL-15[ΔLysM] mice but not in IL-15[ΔCD11c] mice (Figure S5H). These results suggest that memory-phenotype CD8 T cells and vNKT cells may depend on the IL-15 produced by DCs and macrophages/monocytes, respectively.

Hematopoietic cell-derived IL-15 is required for the proliferation and maturation of early BM NK cells

Because IL-15[ΔVav] mice have residual early NK cells in the BM, they may be a suitable model to investigate the role of IL-15 in early NK cell development. Therefore, we performed transcriptome analysis of iNK2 cells and iILC1s from IL-15[ΔVav] and control IL-15[flox/KO] mice (Figure S6A). We found that 142 genes were upregulated and 237 genes were downregulated in the iNK2 stage of IL-15[ΔVav] mice (Figure S6B). A Kyoto Encyclopedia of Genes and Genomes (KEGG) pathway analysis showed that the DNA replication-related, cell-cycle-related, apoptosis-related, and NK cell-mediated cytotoxicity-related pathways were enriched in differentially expressed genes (DEGs) (Figure 6A). The cell-cycle- and DNA replication-related genes were reduced in the iNK2 cells from IL-15[ΔVav] mice (Figure 6B). In addition, genes related to NK cell functions, such as *Ifng*, *Grmb*, and killer cell lectin-like receptors, were downregulated in IL-15[ΔVav] mice (Figure 6C). Finally, anti-apoptotic genes, such as *Bcl2* and *Bcl2l1* (Bcl-xL), were downregulated in the iNK2 cells of IL-15[ΔVav] mice (Figure 6D). Consistent with the reduction of *E2f1* and *E2f2* in the iNK2 cells from IL-15[ΔVav] mice, enrichment analysis of TF targets highlighted *E2f1* and *E2f2* targets (Figure 6E). On the other hand, 33 genes were upregulated and 27 genes were downregulated in the iILC1s from IL-15[ΔVav] mice (Figure S6C). iNK2 cells and

iILC1s shared eight upregulated and ten downregulated DEGs, including *E2f1*, *Grmb*, and *Klra1* (Figure S6D). Thus, these results suggest that the effects of IL-15 on iILC1s are similar to those on iNK2 cells but to a much lesser extent.

To confirm the results of the RNA-seq analysis, we analyzed the proliferation of NK cells. The frequency of bromodeoxyuridine[+] (BrdU^{+}) NK cells was significantly higher in the BM than in the spleen and lung in WT mice (Figure S6E). In addition, BM iNK2 cells showed a higher BrdU incorporation than NK cells at other stages and in other organs (Figure S6F). Thus, these results suggest that the BM is the major site of NK cell development. Next, we analyzed the effect of IL-15 deficiency on NK cell proliferation. BrdU^{+} iNK2 cells were significantly reduced in the BM of IL-15[ΔVav] mice (Figures 6F and 6G). Next, we examined the apoptosis of NK cells by annexin V staining. There was no significant change in annexin V[+]/PI[−] early apoptotic and annexin V[+]/PI[+] late apoptotic populations between IL-15[ΔVav] and control mice (Figures 6H, 6I, and S6G). These results suggest that IL-15 produced by hematopoietic cells supports the proliferation and maturation of early NK cells in the BM.

It is still unclear how IL-15 contributes to the development and maturation of NK cells. To address this question, we analyzed the expression of IL-15-inducible TFs. A comprehensive comparison revealed that *Id2* was significantly reduced, and *Nfil3*, *Tbx21*, *Ikzf3*, and *Klf2* tended to be reduced in IL-15[ΔVav] mice (Figure 6J). Similar to the phenotype of IL-15[ΔVav] mice, it has been reported that NK cell development is arrested at the CD11b^{−} immature NK cell stage in the BM of Id2 KO or NK cell-specific Id2 KO mice.[41–43] Consistent with previous reports that Id2 suppresses *Tcf7* (encoding Tcf1) expression by inhibiting E2A activity,[41–43] *Tcf7* was upregulated in the iNK2 cells of IL-15[ΔVav] mice (Figures 6J and 6K). In addition, several E2A-inducible genes, such as *Cxcr5* and *Il10*, were upregulated in the iNK2 cells of IL-15[ΔVav] mice, whereas T cell lineage-related genes were unchanged (Figure 6K).

To further elucidate the relationship between IL-15 and TFs, we reanalyzed the published RNA-seq data on NK cells from Id2 KO mice and Stat5a[KO/KO];Stat5b[KO/wt] (STAT5 KO) mice.[41,44] As previously reported,[41] the top two DEGs in Id2 KO mice were *Id2* and *Tcf7* (Figure S6H). STAT5 KO mice showed a significant downregulation of *Id2* and upregulation of *Tcf7* (Figure S6I). These results suggest that STAT5 activated by IL-15 may induce Id2. We found that 28% of the downregulated DEGs and 49% of the upregulated DEGs in the iNK2 cells of IL-15[ΔVav] mice were common to Id2 KO and STAT5 KO mice (Figure S6J). Among the common DEGs, NK

Figure 5. Monocyte- and DC-derived IL-15 partially contributes to NK cell development in the BM

(A and B) scRNA-seq data of BM cells underwent UMAP analysis (A). The average expression of *IL15* in each cell population assigned in Figure S5A is shown (B).

(C and D) Absolute number (C) and frequency (D) of NK cells at each developmental stage in the BM of CD11c-Cre[+];IL-15[flox/KO] (IL-15[ΔCD11c]) and IL-15[flox/KO] mice (n = 8).

(E and F) Absolute number (E) and frequency (F) of NK cells at each developmental stage in the BM of LysM-Cre[+];IL-15[flox/KO] (IL-15[ΔLysM]) and IL-15[flox/KO] mice (n = 9).

(G and H) Relative cell number of NK cells after co-culture with monocytes, neutrophils, B cells (G), and hematopoietic progenitors (H) sorted from the BM of CD45.2[+] IL-15^{+/+} or IL-15[KO/KO] mice (n = 4). Cell numbers were normalized to the NK-alone culture.

(I) Representative reconstructed 3D confocal images of the femur from Ncr1-Cre[+];Rosa26[tdTomato/+]; CX3CR1[GFP/+] mice. Red, Ncr1-tdTomato; green, CX3CR1-GFP; white, vasculature; blue, DAPI. Scale bars, 50 μm.

(J) Maximum projection images of clustered NK cell regions. Red, Ncr1-tdTomato; green, CX3CR1-GFP; cyan, MHC I-A/I-E. Scale bars, 50 μm.

Data are mean ± SEM with unpaired two-tailed Student's t test (C, D, E, F, G, and H) pooled from 2–8 independent experiments. *p < 0.05; **p < 0.01; ***p < 0.001. Data represent at least five independent experiments with similar results (H and I). See also Figure S5.
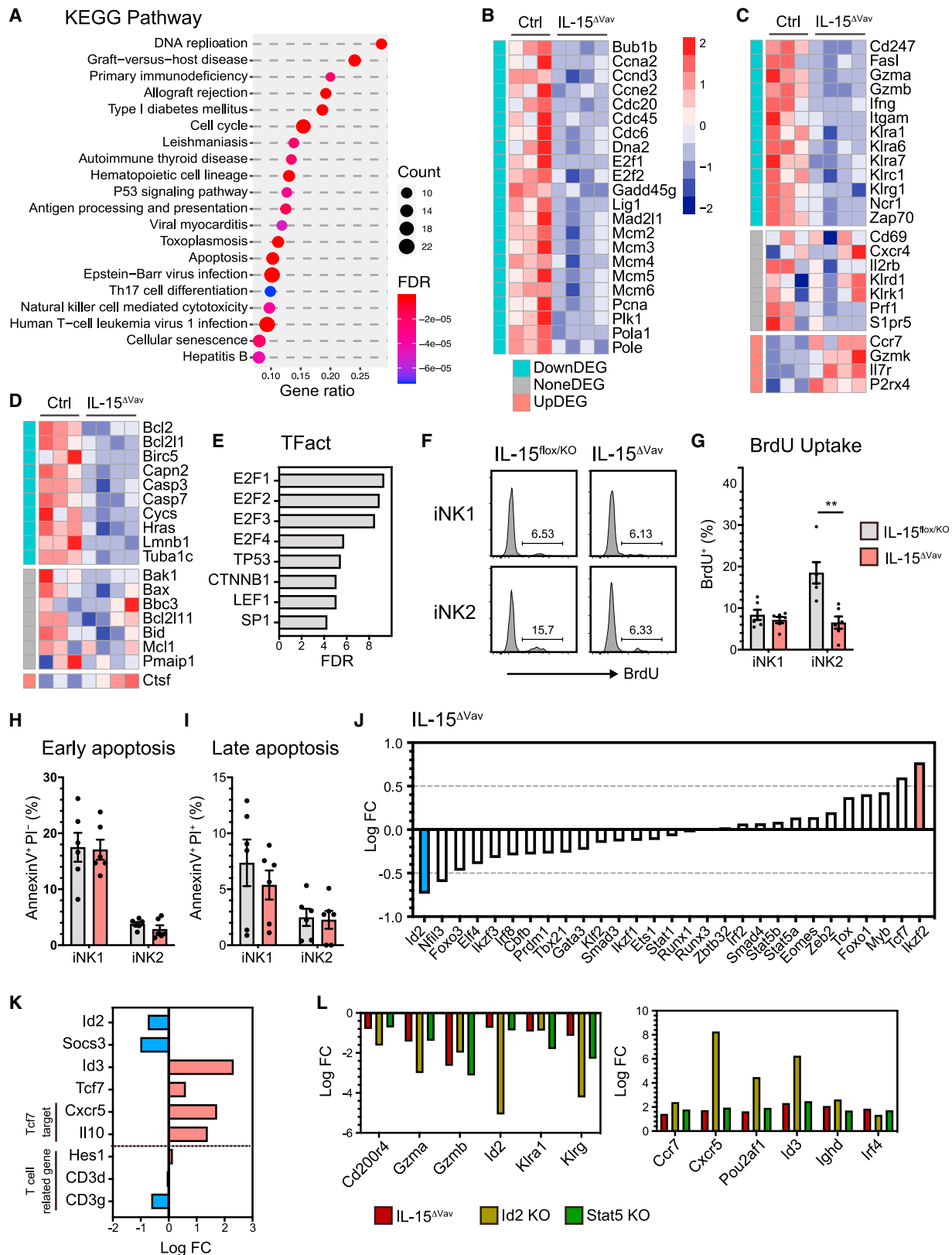
(legend on next page)

cell function-related genes, such as *Gzma* and *Gzmb*, were down-regulated, whereas B cell lineage-related genes, such as *Pou2af1*, *Irf4*, and *Ighd*, were upregulated (Figure 6L). In addition to the T cell lineage genes suppressed by Id2 in NK cells,[41,42] IL-15-induced Id2 may also suppress the expression of B cell lineage-specific genes. Taken together, the IL-15/STAT5/Id2 axis may contribute to cell-fate commitment and maturation during early NK cell development.

Hematopoietic cell-derived IL-15 is required for the maintenance of peripheral NK cells

To evaluate how hematopoietic cell-derived IL-15 affects systemic NK cells, we analyzed the peripheral tissues. Mature NK cells in the spleen and PB were significantly reduced in IL-15$^{\Delta LysM}$ and IL-15$^{\Delta CD11c}$ mice and even more so in IL-15$^{\Delta Vav}$ mice (Figures 7A and 7B), consistent with a previous report on IL-15R$\alpha^{\Delta LysM}$ and IL-15R$\alpha^{\Delta CD11c}$ mice.[18] Notably, mature NK cells in the spleen and PB were significantly reduced in IL-15$^{\Delta LysM}$ and IL-15$^{\Delta CD11c}$ mice, whereas immature NK cells were greatly reduced in IL-15$^{\Delta Vav}$ mice. These results suggest that hematopoietic cell-derived IL-15 may be required to maintain NK cells in the periphery. In contrast, memory-phenotype CD8 T cells and vNKT cells were significantly reduced in the spleen of IL-15$^{\Delta Vav}$ and IL-15$^{\Delta CD11c}$ mice (Figures S7A and S7B), suggesting that these cells are mainly dependent on the IL-15 produced by DCs. Next, we investigated the effect of hematopoietic cell-derived IL-15 on anti-tumor immunity using B16F10 tumor metastasis models. The number of tumor nodules in the lungs was significantly increased in IL-15$^{\Delta Vav}$ mice (Figures 7C and 7D). These results suggest that hematopoietic cell-derived IL-15 is critical for NK cell-mediated anti-tumor immunity.

DISCUSSION

The present study demonstrates that IL-15 produced by mesenchymal stromal cells is dispensable for NK cell development. CAR cells support the maintenance and development of CLPs and early B cells by SCF and IL-7.[25,28,36] Thus, CAR cells are required for NK cell development, at least at the stage of CLPs. However, whether CAR cells play a role in NK cell differentiation after commitment to the NK cell lineage remains unclear. Since rNKPs express c-kit and IL-7R, they may depend on CAR cell-derived SCF and IL-7 for maintenance. After the rNKP stage, iNK cells appear to depend on IL-15 produced by hematopoietic cells. Because iNK cells can quickly encounter myeloid cells in the BM, iNK cells do not need to change their location from

CAR cells. As a result, these iNK cells and their progeny may have a scattered distribution. In contrast, some early NK cells may be attracted to the monocyte and DC clusters by some chemokines, forming the NK cell clusters.

This study found that proliferating early NK cells are present in scattered and clustered fractions. Notably, the NK cell clusters overlap with the accumulation of CX3CR1$^+$ DCs and monocytes. Thus, NK cell clusters may be where NK cell differentiation and maturation occur efficiently with an abundant supply of IL-15. In contrast, proliferating early NK cells in the scattered fraction may receive IL-15 from surrounding myeloid cells. Whether the scattered and clustered NK cells in the BM have different phenotypes or functions remains unclear. Further studies using CXCR4$^{\Delta Ncr1}$ mice are needed to determine the distinct functions of the two types of NK cells in protecting against infection or cancer metastasis. The phenomenon that NK cells differentiate while forming clusters is reminiscent of myelopoiesis clusters that form around specific BECs expressing macrophage colony-stimulating factor.[45] Thus, the development of different hematopoietic cell lineages may occur in clusters.

This study demonstrated that CXCL12/CXCR4 signaling is required for NK cell distribution in the BM. Several CXCL12-producing stromal cells have been reported in the BM. Although CAR/Lepr$^+$ cells are the major CXCL12-producing stromal cells, Lepr-Cre-induced CXCL12 ablation does not affect the frequency or localization of HSCs.[35,36] This is probably because the deletion efficiency of the Lepr-Cre transgene is only 70%–90% of CAR cells, and the remaining CXCL12-producing CAR cells are sufficient to maintain HSCs.[23] It has been reported that arterial endothelial cells and NG2$^+$ peri-arterial pericytes also produce CXCL12.[35,46] Therefore, these stromal cells, including CAR cells, are candidates for the CXCL12 source of HSCs and NK cells in the BM.

We have shown that monocytes are one of the sources of IL-15 required for NK cell development in the BM. *C. albicans* infection strongly induces the expression of IL-15 and IL-15Rα in monocytes to enhance the immune response by NK cells.[47] In addition, influenza virus infection or the administration of Toll-like receptor ligands increases the proliferation of NK cells in the BM.[48,49] Although it is unclear whether IL-15 is involved in the expansion of BM NK cells in inflammation, upregulation of IL-15 from monocytes may promote NK cell differentiation in the BM. Conversely, in *T. gondii* infection, NK cells locally promote monocyte differentiation in the BM by IFN-γ.[50] Thus, it is possible that NK cells and monocytes mutually enhance their

---

Figure 6. IL-15 is required for the proliferation and maturation of NK cells in the BM

(A) The top 20 enriched pathways in KEGG for the set of DEGs (false discovery rate <0.1) in iNK2 cells from the BM of IL-15$^{\Delta Vav}$ and IL-15$^{flox/KO}$ mice.

(B–D) Heatmaps showing the expression of genes related to cell cycle or DNA replication (B), NK cell function (C), and apoptosis (D) in iNK2 cells from the BM of IL-15$^{\Delta Vav}$ and IL-15$^{flox/KO}$ mice.

(E) Enrichment analysis of transcriptional targets of the DEGs in iNK2 cells using the TFact database.

(F and G) Representative FCM plots (F) and frequency (G) of BrdU$^+$ iNK1 and iNK2 cells in the BM from IL-15$^{\Delta Vav}$ and IL-15$^{flox/KO}$ mice (n = 6).

(H and I) Frequency of PI$^-$annexin V$^+$ early apoptotic (H) and PI$^+$annexin V$^+$ late apoptotic (I) cells in the indicated NK cell subset in the BM of IL-15$^{\Delta Vav}$ and IL-15$^{flox/KO}$ mice (n = 6).

(J and K) Fold change in the expression of transcription factors associated with NK cells (J) and E2A target genes and T cell lineage-related genes (K) in IL-15$^{\Delta Vav}$ mice relative to those in IL-15$^{flox/KO}$ mice.

(L) Fold change of overlapping DEGs between IL-15$^{\Delta Vav}$, Id2 KO, and STAT5 KO mice.

Data are mean ± SEM with unpaired two-tailed Student's t test (G, H, and I) pooled from 2–6 independent experiments. **p < 0.01. Data represent at least six independent experiments with similar results (F). See also Figure S6.
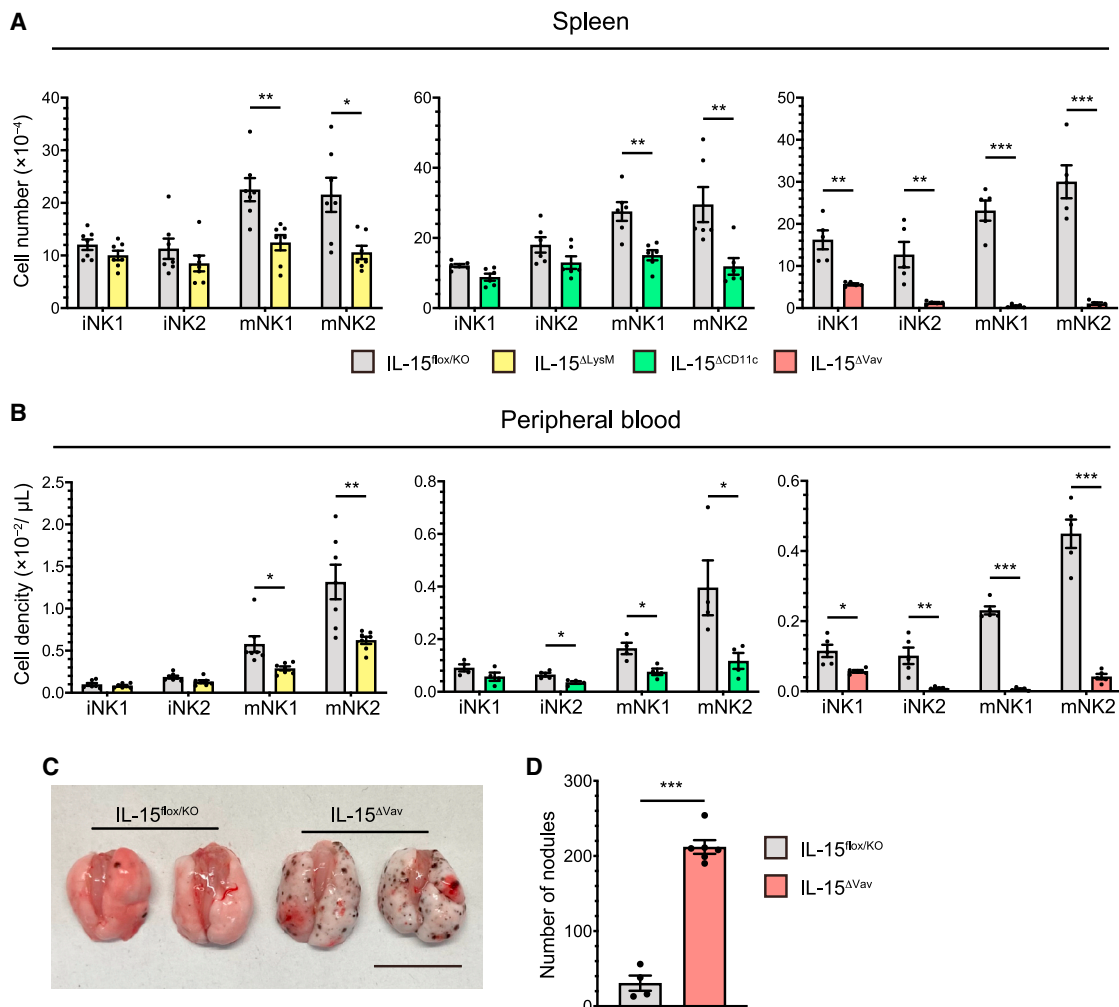
Figure 7. Hematopoietic cell-derived IL-15 is essential for NK cell maintenance in the periphery

(A and B) Absolute numbers of NK cells at each developmental stage in the spleen (A) and peripheral blood (B) of the indicated mice (n = 5–7).

(C and D) IL-15$^{\Delta Vav}$ and IL-15$^{flox/KO}$ mice were injected with 5 × 10^4 B16F10 melanoma cells. Lung metastasis (C) and the number of metastatic nodules (D) in the lung at 12 days are shown (n = 4–6). Scale bar, 1 cm.

Data are mean ± SEM with unpaired two-tailed Student's t test (A, B, and D) and pooled from 2–7 independent experiments. *p < 0.05; **p < 0.01; ***p < 0.001. Data represent at least two independent experiments with similar results (C). See also Figure S7.

differentiation in the BM during inflammation. On the other hand, we conclude that BM stromal cell-derived IL-15 is not required for NK cell differentiation under normal conditions. However, the possibility remains that BM stromal cell-derived IL-15 may promote NK cell differentiation during inflammation and infection. Elucidating the role of BM IL-15 in hematopoiesis in health and inflammation is an interesting question for the future.

We found that IL-15 produced by hematopoietic cells promotes the proliferation of immature NK cells. In contrast, IL-15 in peripheral tissues supports the survival of NK cells in transfer experiments. There are two possible explanations for the different responses of NK cells in the BM and periphery. First, the high proliferative capacity of immature NK cells may have led to the result that IL-15 has a predominant effect on their proliferation. Second, IL-15 at higher concentrations predominantly

activates the PI3K/Akt/mTOR pathway over the STAT5 pathway and promotes NK cell proliferation.[51] Thus, IL-15 may play a dominant role in the expansion of early NK cells in the BM due to the abundance of IL-15.

Limitations of the study

This study used different Cre driver mouse lines to analyze the cellular source of IL-15. In particular, the specificity of the LysM-Cre and CD11c-Cre mice was not perfect, being expressed in many immune cell types with a wide range of efficiencies, making interpretation of the results difficult. Recently, Ms4a3-Cre mice have been developed that specifically and efficiently target monocytes and granulocytes,[52] which may allow a more specific analysis of the role of monocyte-derived IL-15 in NK cell differentiation.

STAR★METHODS

Detailed methods are provided in the online version of this paper and include the following:

- KEY RESOURCES TABLE
- RESOURCE AVAILABILITY
  - Lead contact
  - Materials availability
  - Data and code availability
- EXPERIMENTAL MODEL AND STUDY PARTICIPANT DETAILS
  - Mice
- METHOD DETAILS
  - Cell isolation
  - Flow cytometry and cell sorting
  - BrdU incorporation
  - Cell culture
  - Bone marrow transplantation
  - Real-time RT-qPCR
  - Immunofluorescence analysis
  - Tissue clearing and deep imaging of bone marrow
  - RNA preparation and next-generation sequencing
  - scRNA-seq analysis
- QUANTIFICATION AND STATISTICAL ANALYSIS

AUTHOR CONTRIBUTIONS

Conceptualization, S.A. and K.I.; methodology, S.A.; formal analysis, S.A., N.N., R.Y., K.M., M.M., and A.V.; investigation, S.A., T.A., T.H., G.C., A.S., S.T., K.Y., H.M., and S.K.; resources, J.K., M.I., T.O., V.S., and T.N.; writing – original draft, S.A. and K.I.; writing – review & editing, S.A. and K.I.; funding acquisition, K.I., T.H., G.C., A.S., T.A., and S.T.; supervision, K.I.

DECLARATION OF INTERESTS

The authors declare no competing interests.

INCLUSION AND DIVERSITY

We support inclusive, diverse, and equitable conduct of research.

REFERENCES

1. Eberl, G., Colonna, M., Di Santo, J.P., and McKenzie, A.N.J. (2015). Innate lymphoid cells: a new paradigm in immunology. Science 348, aaa6566. https://doi.org/10.1126/science.aaa6566.

2. Vivier, E., Artis, D., Colonna, M., Diefenbach, A., Di Santo, J.P., Eberl, G., Koyasu, S., Locksley, R.M., McKenzie, A.N.J., Mebius, R.E., et al. (2018). Innate lymphoid cells: 10 years on. Cell 174, 1054–1066. https://doi.org/10.1016/j.cell.2018.07.017.

3. Fuchs, A., Vermi, W., Lee, J.S., Lonardi, S., Gilfillan, S., Newberry, R.D., Cella, M., and Colonna, M. (2013). Intraepithelial type 1 innate lymphoid cells are a unique subset of IL-12- and IL-15-responsive IFN-γ-producing cells. Immunity 38, 769–781. https://doi.org/10.1016/j.immuni.2013.02.010.

4. Bernink, J.H., Peters, C.P., Munneke, M., te Velde, A.A., Meijer, S.L., Weijer, K., Hreggvidsdottir, H.S., Heinsbroek, S.E., Legrand, N., Buskens, C.J., et al. (2013). Human type 1 innate lymphoid cells accumulate in inflamed mucosal tissues. Nat. Immunol. 14, 221–229. https://doi.org/10.1038/ni.2534.

5. Sojka, D.K., Plougastel-Douglas, B., Yang, L., Pak-Wittel, M.A., Artyomov, M.N., Ivanova, Y., Zhong, C., Chase, J.M., Rothman, P.B., Yu, J., et al. (2014). Tissue-resident natural killer (NK) cells are cell lineages distinct from thymic and conventional splenic NK cells. Elife 3, e01659. https://doi.org/10.7554/eLife.01659.

6. Cortez, V.S., and Colonna, M. (2016). Diversity and function of group 1 innate lymphoid cells. Immunol. Lett. 179, 19–24. https://doi.org/10.1016/j.imlet.2016.07.005.

7. Daussy, C., Faure, F., Mayol, K., Viel, S., Gasteiger, G., Charrier, E., Bienvenu, J., Henry, T., Debien, E., Hasan, U.A., et al. (2014). T-bet and Eomes instruct the development of two distinct natural killer cell lineages in the liver and in the bone marrow. J. Exp. Med. 211, 563–577. https://doi.org/10.1084/jem.20131560.

8. Klose, C.S.N., Flach, M., Möhle, L., Rogell, L., Hoyler, T., Ebert, K., Fabiunke, C., Pfeifer, D., Sexl, V., Fonseca-Pereira, D., et al. (2014). Differentiation of type 1 ILCs from a common progenitor to all helper-like innate lymphoid cell lineages. Cell 157, 340–356. https://doi.org/10.1016/j.cell.2014.03.030.

9. Diefenbach, A., Colonna, M., and Koyasu, S. (2014). Development, differentiation, and diversity of innate lymphoid cells. Immunity 41, 354–365. https://doi.org/10.1016/j.immuni.2014.09.005.

10. Goh, W., and Huntington, N.D. (2017). Regulation of murine natural killer cell development. Front. Immunol. 8, 130. https://doi.org/10.3389/fimmu.2017.00130.

11. Held, W., Jeevan-Raj, B., and Charmoy, M. (2018). Transcriptional regulation of murine natural killer cell development, differentiation and maturation. Cell. Mol. Life Sci. 75, 3371–3379. https://doi.org/10.1007/s00018-018-2865-1.

12. Brillantes, M., and Beaulieu, A.M. (2019). Transcriptional control of natural killer cell differentiation. Immunology 156, 111–119. https://doi.org/10.1111/imm.13017.

13. Lodolce, J.P., Boone, D.L., Chai, S., Swain, R.E., Dassopoulos, T., Trettin, S., and Ma, A. (1998). IL-15 receptor maintains lymphoid homeostasis by supporting lymphocyte homing and proliferation. Immunity 9, 669–676. https://doi.org/10.1016/s1074-7613(00)80664-0.

14. Kennedy, M.K., Glaccum, M., Brown, S.N., Butz, E.A., Viney, J.L., Embers, M., Matsuki, N., Charrier, K., Sedger, L., Willis, C.R., et al. (2000). Reversible defects in natural killer and memory CD8 T cell lineages in interleukin 15-deficient mice. J. Exp. Med. 191, 771–780. https://doi.org/10.1084/jem.191.5.771.

15. Dubois, S., Mariner, J., Waldmann, T.A., and Tagaya, Y. (2002). IL-15Rα recycles and presents IL-15 in trans to neighboring cells. Immunity 17, 537–547. https://doi.org/10.1016/s1074-7613(02)00429-6.

16. Burkett, P.R., Koka, R., Chien, M., Chai, S., Boone, D.L., and Ma, A. (2004). Coordinate expression and trans presentation of interleukin (IL)-15Rα and IL-15 supports natural killer cell and memory CD8+ T cell homeostasis. J. Exp. Med. 200, 825–834. https://doi.org/10.1084/jem.20041389.

17. Mortier, E., Woo, T., Advincula, R., Gozalo, S., and Ma, A. (2008). IL-15Rα chaperones IL-15 to stable dendritic cell membrane complexes that activate NK cells via trans presentation. J. Exp. Med. 205, 1213–1225. https://doi.org/10.1084/jem.20071913.

18. Mortier, E., Advincula, R., Kim, L., Chmura, S., Barrera, J., Reizis, B., Malynn, B.A., and Ma, A. (2009). Macrophage- and dendritic-cell-derived interleukin-15 receptor alpha supports homeostasis of distinct CD8+ T cell subsets. Immunity 31, 811–822. https://doi.org/10.1016/j.immuni.2009.09.017.

19. Zhu, Y., Cui, G., Miyauchi, E., Nakanishi, Y., Mukohira, H., Shimba, A., Abe, S., Tani-ichi, S., Hara, T., Nakase, H., et al. (2020). Intestinal epithelial cell-derived IL-15 determines local maintenance and maturation of intraepithelial lymphocytes in the intestine. Int. Immunol. 32, 307–319. https://doi.org/10.1093/intimm/dxz082.

20. Cepero-Donates, Y., Rakotoarivelo, V., Mayhue, M., Ma, A., Chen, Y.G., and Ramanathan, S. (2016). Homeostasis of IL-15 dependent lymphocyte subsets in the liver. Cytokine 82, 95–101. https://doi.org/10.1016/j.cyto.2015.12.012.

21. Liou, Y.H., Wang, S.W., Chang, C.L., Huang, P.L., Hou, M.S., Lai, Y.G., Lee, G.A., Jiang, S.T., Tsai, C.Y., and Liao, N.S. (2014). Adipocyte IL-15 regulates local and systemic NK cell development. J. Immunol. 193, 1747–1758. https://doi.org/10.4049/jimmunol.1400868.

22. Tao, H., Li, L., Liao, N.S., Schluns, K.S., Luckhart, S., Sleasman, J.W., and Zhong, X.P. (2021). Thymic epithelial cell-derived IL-15 and IL-15 receptor α chain foster local environment for type 1 innate like T cell development. Front. Immunol. 12, 623280. https://doi.org/10.3389/fimmu.2021.623280.

23. Sugiyama, T., Omatsu, Y., and Nagasawa, T. (2019). Niches for hematopoietic stem cells and immune cell progenitors. Int. Immunol. 31, 5–11. https://doi.org/10.1093/intimm/dxy058.

24. Omatsu, Y., Sugiyama, T., Kohara, H., Kondoh, G., Fujii, N., Kohno, K., and Nagasawa, T. (2010). The essential functions of adipo-osteogenic progenitors as the hematopoietic stem and progenitor cell niche. Immunity 33, 387–399. https://doi.org/10.1016/j.immuni.2010.08.017.

25. Cordeiro Gomes, A., Hara, T., Lim, V.Y., Herndler-Brandstetter, D., Nevius, E., Sugiyama, T., Tani-ichi, S., Schlenner, S., Richie, E., Rodewald, H.R., et al. (2016). Hematopoietic stem cell niches produce lineage-instructive signals to control multipotent progenitor differentiation. Immunity 45, 1219–1231. https://doi.org/10.1016/j.immuni.2016.11.004.

26. Greenbaum, A., Hsu, Y.M.S., Day, R.B., Schuettpelz, L.G., Christopher, M.J., Borgerding, J.N., Nagasawa, T., and Link, D.C. (2013). CXCL12 in early mesenchymal progenitors is required for haematopoietic stem-cell maintenance. Nature 495, 227–230. https://doi.org/10.1038/nature11926.

27. Ding, L., Saunders, T.L., Enikolopov, G., and Morrison, S.J. (2012). Endothelial and perivascular cells maintain haematopoietic stem cells. Nature 481, 457–462. https://doi.org/10.1038/nature10783.

28. Comazzetto, S., Murphy, M.M., Berto, S., Jeffery, E., Zhao, Z., and Morrison, S.J. (2019). Restricted hematopoietic progenitors and erythropoiesis eequire SCF from leptin receptor+ niche cells in the bone marrow. Cell Stem Cell 24, 477–486.e6. https://doi.org/10.1016/j.stem.2018.11.022.

29. Noda, M., Omatsu, Y., Sugiyama, T., Oishi, S., Fujii, N., and Nagasawa, T. (2011). CXCL12-CXCR4 chemokine signaling is essential for NK-cell development in adult mice. Blood 117, 451–458. https://doi.org/10.1182/blood-2010-04-277897.

30. Cui, G., Hara, T., Simmons, S., Wagatsuma, K., Abe, A., Miyachi, H., Kitano, S., Ishii, M., Tani-ichi, S., and Ikuta, K. (2014). Characterization of the IL-15 niche in primary and secondary lymphoid organs in vivo. Proc. Natl. Acad. Sci. USA 111, 1915–1920. https://doi.org/10.1073/pnas.1318281111.

31. Colpitts, S.L., Stonier, S.W., Stoklasek, T.A., Root, S.H., Aguila, H.L., Schluns, K.S., and Lefrançois, L. (2013). Transcriptional regulation of IL-15 expression during hematopoiesis. J. Immunol. 191, 3017–3024. https://doi.org/10.4049/jimmunol.1301389.

32. Susaki, E.A., Tainaka, K., Perrin, D., Kishino, F., Tawara, T., Watanabe, T.M., Yokoyama, C., Onoe, H., Eguchi, M., Yamaguchi, S., et al. (2014). Whole-brain imaging with single-cell resolution using chemical cocktails and computational analysis. Cell 157, 726–739. https://doi.org/10.1016/j.cell.2014.03.042.

33. Walzer, T., Chiossone, L., Chaix, J., Calver, A., Carozzo, C., Garrigue-Antar, L., Jacques, Y., Baratin, M., Tomasello, E., and Vivier, E. (2007). Natural killer cell trafficking in vivo requires a dedicated sphingosine 1-phosphate receptor. Nat. Immunol. 8, 1337–1344. https://doi.org/10.1038/ni1523.

34. Baryawno, N., Przybylski, D., Kowalczyk, M.S., Kfoury, Y., Severe, N., Gustafsson, K., Kokkaliaris, K.D., Mercier, F., Tabaka, M., Hofree, M., et al. (2019). A cellular taxonomy of the bone marrow stroma in homeostasis and leukemia. Cell 177, 1915–1932.e16. https://doi.org/10.1016/j.cell.2019.04.040.

35. Asada, N., Kunisaki, Y., Pierce, H., Wang, Z., Fernandez, N.F., Birbrair, A., Ma'ayan, A., and Frenette, P.S. (2017). Differential cytokine contributions of perivascular haematopoietic stem cell niches. Nat. Cell Biol. 19, 214–223. https://doi.org/10.1038/ncb3475.

36. Ding, L., and Morrison, S.J. (2013). Haematopoietic stem cells and early lymphoid progenitors occupy distinct bone marrow niches. Nature 495, 231–235. https://doi.org/10.1038/nature11885.

37. Mayol, K., Biajoux, V., Marvel, J., Balabanian, K., and Walzer, T. (2011). Sequential desensitization of CXCR4 and S1P5 controls natural killer cell trafficking. Blood 118, 4863–4871. https://doi.org/10.1182/blood-2011-06-362574.

38. Sciumè, G., De Angelis, G., Benigni, G., Ponzetta, A., Morrone, S., Santoni, A., and Bernardini, G. (2011). CX3CR1 expression defines 2 KLRG1+ mouse NK-cell subsets with distinct functional properties and positioning in the bone marrow. Blood 117, 4467–4475. https://doi.org/10.1182/blood-2010-07-297101.

39. Bernardini, G., Sciumè, G., Bosisio, D., Morrone, S., Sozzani, S., and Santoni, A. (2008). CCL3 and CXCL12 regulate trafficking of mouse bone marrow NK cell subsets. Blood 111, 3626–3634. https://doi.org/10.1182/blood-2007-08-106203.

40. Tabula Muris Consortium; Overall coordination; Logistical coordination; Organ collection and processing; Library preparation and sequencing; Computational data analysis; Cell type annotation; Writing group; Supplemental text writing group; Principal investigators (2018). Single-cell transcriptomics of 20 mouse organs creates a Tabula Muris. Nature 562, 367–372. https://doi.org/10.1038/s41586-018-0590-4.

41. Delconte, R.B., Shi, W., Sathe, P., Ushiki, T., Seillet, C., Minnich, M., Kolesnik, T.B., Rankin, L.C., Mielke, L.A., Zhang, J.G., et al. (2016). The helix-loop-helix protein ID2 governs NK cell fate by tuning their sensitivity to interleukin-15. Immunity 44, 103–115. https://doi.org/10.1016/j.immuni.2015.12.007.

42. Zook, E.C., Li, Z.Y., Xu, Y., de Pooter, R.F., Verykokakis, M., Beaulieu, A., Lasorella, A., Maienschein-Cline, M., Sun, J.C., Sigvardsson, M., and Kee, B.L. (2018). Transcription factor ID2 prevents E proteins from enforcing a naive T lymphocyte gene program during NK cell development. Sci. Immunol. 3, eaao2139. https://doi.org/10.1126/sciimmunol.aao2139.

43. Li, Z.Y., Morman, R.E., Hegermiller, E., Sun, M., Bartom, E.T., Maienschein-Cline, M., Sigvardsson, M., and Kee, B.L. (2021). The transcriptional repressor ID2 supports natural killer cell maturation by controlling TCF1 amplitude. J. Exp. Med. 218, e20202032. https://doi.org/10.1084/jem.20202032.

44. Villarino, A.V., Sciumè, G., Davis, F.P., Iwata, S., Zitti, B., Robinson, G.W., Hennighausen, L., Kanno, Y., and O'Shea, J.J. (2017). Subset- and tissue-defined STAT5 thresholds control homeostasis and function of innate

lymphoid cells. J. Exp. Med. *214*, 2999–3014. https://doi.org/10.1084/jem.20150907.

45. Zhang, J., Wu, Q., Johnson, C.B., Pham, G., Kinder, J.M., Olsson, A., Slaughter, A., May, M., Weinhaus, B., D'Alessandro, A., et al. (2021). In situ mapping identifies distinct vascular niches for myelopoiesis. Nature *590*, 457–462. https://doi.org/10.1038/s41586-021-03201-2.

46. Xu, C., Gao, X., Wei, Q., Nakahara, F., Zimmerman, S.E., Mar, J., and Frenette, P.S. (2018). Stem cell factor is selectively secreted by arterial endothelial cells in bone marrow. Nat. Commun. *9*, 2449. https://doi.org/10.1038/s41467-018-04726-3.

47. Domínguez-Andrés, J., Feo-Lucas, L., Minguito de la Escalera, M., González, L., López-Bravo, M., and Ardavín, C. (2017). Inflammatory Ly6C^{high} monocytes protect against Candidiasis through IL-15-driven NK cell/neutrophil activation. Immunity *46*, 1059–1072.e4. https://doi.org/10.1016/j.immuni.2017.05.009.

48. van Helden, M.J.G., de Graaf, N., Boog, C.J.P., Topham, D.J., Zaiss, D.M.W., and Sijts, A.J.A.M. (2012). The bone marrow functions as the central site of proliferation for long-lived NK cells. J. Immunol. *189*, 2333–2337. https://doi.org/10.4049/jimmunol.1200008.

49. Milo, I., Blecher-Gonen, R., Barnett-Itzhaki, Z., Bar-Ziv, R., Tal, O., Gurevich, I., Feferman, T., Drexler, I., Amit, I., Bousso, P., and Shakhar, G. (2018). The bone marrow is patrolled by NK cells that are primed and expand in response to systemic viral activation. Eur. J. Immunol. *48*, 1137–1152. https://doi.org/10.1002/eji.201747378.

50. Askenase, M.H., Han, S.J., Byrd, A.L., Morais da Fonseca, D., Bouladoux, N., Wilhelm, C., Konkel, J.E., Hand, T.W., Lacerda-Queiroz, N., Su, X.Z., et al. (2015). Bone-marrow-resident NK cells prime monocytes for regulatory function during infection. Immunity *42*, 1130–1142. https://doi.org/10.1016/j.immuni.2015.05.011.

51. Marçais, A., Cherfils-Vicini, J., Viant, C., Degouve, S., Viel, S., Fenis, A., Rabilloud, J., Mayol, K., Tavares, A., Bienvenu, J., et al. (2014). The metabolic checkpoint kinase mTOR is essential for IL-15 signaling during the development and activation of NK cells. Nat. Immunol. *15*, 749–757. https://doi.org/10.1038/ni.2936.

52. Liu, Z., Gu, Y., Chakarov, S., Bleriot, C., Kwok, I., Chen, X., Shin, A., Huang, W., Dress, R.J., Dutertre, C.A., et al. (2019). Fate mapping via Ms4a3-expression history traces monocyte-derived cells. Cell *178*, 1509–1525.e19. https://doi.org/10.1016/j.cell.2019.08.009.

53. Cui, G., Shimba, A., Jin, J., Ogawa, T., Muramoto, Y., Miyachi, H., Abe, S., Asahi, T., Tani-Ichi, S., Dijkstra, J.M., et al. (2022). A circulating subset of iNKT cells mediates antitumor and antiviral immunity. Sci. Immunol. *7*, eabj8760. https://doi.org/10.1126/sciimmunol.abj8760.

54. Schindelin, J., Arganda-Carreras, I., Frise, E., Kaynig, V., Longair, M., Pietzsch, T., Preibisch, S., Rueden, C., Saalfeld, S., Schmid, B., et al. (2012). Fiji: an open-source platform for biological-image analysis. Nat. Methods *9*, 676–682. https://doi.org/10.1038/nmeth.2019.

55. Bolger, A.M., Lohse, M., and Usadel, B. (2014). Trimmomatic: a flexible trimmer for Illumina sequence data. Bioinformatics *30*, 2114–2120. https://doi.org/10.1093/bioinformatics/btu170.

56. Kim, D., Langmead, B., and Salzberg, S.L. (2015). HISAT: a fast spliced aligner with low memory requirements. Nat. Methods *12*, 357–360. https://doi.org/10.1038/nmeth.3317.

57. Liao, Y., Smyth, G.K., and Shi, W. (2014). featureCounts: an efficient general purpose program for assigning sequence reads to genomic features. Bioinformatics *30*, 923–930. https://doi.org/10.1093/bioinformatics/btt656.

58. Robinson, M.D., McCarthy, D.J., and Smyth, G.K. (2010). edgeR: a Bioconductor package for differential expression analysis of digital gene expression data. Bioinformatics *26*, 139–140. https://doi.org/10.1093/bioinformatics/btp616.

59. Stuart, T., Butler, A., Hoffman, P., Hafemeister, C., Papalexi, E., Mauck, W.M., 3rd, Hao, Y., Stoeckius, M., Smibert, P., and Satija, R. (2019). Comprehensive integration of single-cell data. Cell *177*, 1888–1902.e21. https://doi.org/10.1016/j.cell.2019.05.031.

60. Ge, S.X., Jung, D., and Yao, R. (2020). ShinyGO: a graphical gene-set enrichment tool for animals and plants. Bioinformatics *36*, 2628–2629. https://doi.org/10.1093/bioinformatics/btz931.

61. Caton, M.L., Smith-Raska, M.R., and Reizis, B. (2007). Notch-RBP-J signaling controls the homeostasis of CD8⁻ dendritic cells in the spleen. J. Exp. Med. *204*, 1653–1664. https://doi.org/10.1084/jem.20062648.

62. Jung, S., Aliberti, J., Graemmel, P., Sunshine, M.J., Kreutzberg, G.W., Sher, A., and Littman, D.R. (2000). Analysis of fractalkine receptor CX$_3$CR1 function by targeted deletion and green fluorescent protein reporter gene insertion. Mol. Cell Biol. *20*, 4106–4114. https://doi.org/10.1128/mcb.20.11.4106-4114.2000.

63. DeFalco, J., Tomishima, M., Liu, H., Zhao, C., Cai, X., Marth, J.D., Enquist, L., and Friedman, J.M. (2001). Virus-assisted mapping of neural inputs to a feeding center in the hypothalamus. Science *291*, 2608–2613. https://doi.org/10.1126/science.1056602.

64. Madisen, L., Zwingman, T.A., Sunkin, S.M., Oh, S.W., Zariwala, H.A., Gu, H., Ng, L.L., Palmiter, R.D., Hawrylycz, M.J., Jones, A.R., et al. (2010). A robust and high-throughput Cre reporting and characterization system for the whole mouse brain. Nat. Neurosci. *13*, 133–140. https://doi.org/10.1038/nn.2467.

65. Logan, M., Martin, J.F., Nagy, A., Lobe, C., Olson, E.N., and Tabin, C.J. (2002). Expression of Cre recombinase in the developing mouse limb bud driven by a *Prxl* enhancer. Genesis *33*, 77–80. https://doi.org/10.1002/gene.10092.

66. Tokoyoda, K., Egawa, T., Sugiyama, T., Choi, B.I., and Nagasawa, T. (2004). Cellular niches controlling B lymphocyte behavior within bone marrow during development. Immunity *20*, 707–718. https://doi.org/10.1016/j.immuni.2004.05.001.

67. Ara, T., Itoi, M., Kawabata, K., Egawa, T., Tokoyoda, K., Sugiyama, T., Fujii, N., Amagai, T., and Nagasawa, T. (2003). A role of CXC chemokine ligand 12/stromal cell-derived factor-1/pre-B cell growth stimulating factor and its receptor CXCR4 in fetal and adult T cell development in vivo. J. Immunol. *170*, 4649–4655. https://doi.org/10.4049/jimmunol.170.9.4649.

68. Kisanuki, Y.Y., Hammer, R.E., Miyazaki, J., Williams, S.C., Richardson, J.A., and Yanagisawa, M. (2001). Tie2-Cre transgenic mice: a new model for endothelial cell-lineage analysis in vivo. Dev. Biol. *230*, 230–242. https://doi.org/10.1006/dbio.2000.0106.

69. Eckelhart, E., Warsch, W., Zebedin, E., Simma, O., Stoiber, D., Kolbe, T., Rülicke, T., Mueller, M., Casanova, E., and Sexl, V. (2011). A novel Ncr1-Cre mouse reveals the essential role of STAT5 for NK-cell survival and development. Blood *117*, 1565–1573. https://doi.org/10.1182/blood-2010-06-291633.

70. Stadtfeld, M., and Graf, T. (2005). Assessing the role of hematopoietic plasticity for endothelial and hepatocyte development by non-invasive lineage tracing. Development *132*, 203–213. https://doi.org/10.1242/dev.01558.

71. Kawamoto, T., and Shimizu, M. (2000). A method for preparing 2- to 50-micron-thick fresh-frozen sections of large samples and undecalcified hard tissues. Histochem. Cell Biol. *113*, 331–339. https://doi.org/10.1007/s004180000149.

Cell Reports
Article

STAR★METHODS

KEY RESOURCES TABLE

REAGENT or RESOURCE	SOURCE	IDENTIFIER
Antibodies		
Anti-mouse CD3ε PE-Cy7 (145-2C11)	ThermoFisher Scientific	Cat#25-0031-82; RRID:AB_469572
Anti-mouse CD3ε APC-Cy7 (145-2C11)	BioLegend	Cat#100330; RRID:AB_1877170
Anti-mouse CD3ε FITC (145-2C11)	BioLegend	Cat#100306; RRID:AB_312671
Anti-mouse NK1.1 APC (PK136)	BioLegend	Cat#108710; RRID:AB_313397
Anti-mouse CD127 Biotin (A7R34)	BioLegend	Cat#135006; RRID:AB_2126118
Anti-mouse CD127 PE (A7R34)	Biolegend	Cat#135010; RRID:AB_1937251
Anti-Rat/Mouse CD49a PE (Ha31/8)	BD Biosciences	Cat#562115; RRID:AB_11153117
Anti-muse CD49b FITC (DX5)	BioLegend	Cat#108906; RRID:AB_313413
Anti-mouse CD27 APC-eFluor780 (LG.7F9)	ThermoFisher Scientific	Cat#47-0271-82; RRID:AB_10853642
Anti-mouse/human CD11b BV510 (M1/70)	Biolegend	Cat#101263; RRID:AB_2629529
Anti-mouse/human CD11 b PE (M1/70)	BioLegend	Cat#101207; RRID:AB_312790
Anti-mouse CD335/Nkp46 PE-Cy7 (29A1.4)	BioLegend	Cat#137618; RRID:AB_11219186
Anti-mouse EOMES PE (Dan11mag)	ThermoFisher Scientific	Cat#12-4875-82; RRID:AB_1603275
Anti-mouse TCRβ FITC (H57-597)	BioLegend	Cat#109206; RRID:AB_313429
Anti-mouse TCRβ Biotin (H57-597)	BioLegend	Cat#109204; RRID:AB_313427
Aiti-mouse CD4 FITC (GK1.5)	BioLegend	Cat#100406; RRID:AB_312691
Aiti-mouse CD4 APC-eFluor780 (RM4-5)	ThermoFisher Scientific	Cat#47-0042-82; RRID:AB_1272183
Anti-mouse CD8α FITC (53–6.7)	BioLegend	Cat#100706; RRID:AB_312745
Anti-mouse CD8α PE (53–6.7)	BioLegend	Cat#100708; RRID:AB_312747
Anti-human/mouse CD44 PE-Cy7 (IM7)	ThermoFisher Scientific	Cat#25-0441-82; RRID:AB_469623
Anti-human/mouse CD45R/B220 FITC (RA3-6B2)	BioLegend	Cat#103206; RRID:AB_312991
Anti-mouse CD19 Alexa Fluor 488 (6D5)	BioLegend	Cat#115521; RRID:AB_389307
Anti-mouse CD45 APC-Cy7 (30-F11)	BioLegend	Cat#103116; RRID:AB_312981
Anti-mouse CD45.1 BV510 (A20)	BioLegend	Cat#110741; RRID:AB_2563378
Anti-mouse CD45.2 PerCP-Cy5.5 (104)	BioLegend	Cat#109828; RRID:AB_893350
Anti-mouse CD122 Biotin (TM-β1)	BioLegend	Cat#123206; RRID:AB_940609
Anti-mouse CD244.2/2B4 PE-Cy7 (eBio244F4)	ThermoFisher Scientific	Cat#25-2441-82; RRID:AB_2573432
Anti-mouse CD135/Flt3 PE (A2F10)	BioLegend	Cat#135306; RRID:AB_1877217
Anti-mouse CD135/Flt3 BV421 (A2F10)	BioLegend	Cat#135315; RRID:AB_2571919
Anti-mouse CD279/PD-1 BV421 (29F.1A12)	BioLegend	Cat#135221; RRID:AB_2562568
Anti-mouse CD25 APC-Cy7 (PC61)	BioLegend	Cat#102026; RRID:AB_830745
Anti-mouse CD11c FITC (N418)	ThermoFisher Scientific	Cat#11-0114-82; RRID:AB_464940
Anti-mouse FcεRIα FITC (MAR-1)	BioLegend	Cat#134306; RRID:1626108
Anti-mouse Ly-6D FITC (49-H4)	BioLegend	Cat#138606; RRID:AB_11203888
Anti-mouse TER-119 FITC (TER-119)	BioLegend	Cat#116206; RRID:AB_313707
Anti-mouse CD115/CSF-1R Biotin (AFS98)	BioLegend	Cat#135507; RRID:AB_2028401
Anti-mouse Gr-1 FITC (RB6-8C5)	BioLegend	Cat#108406; RRID:AB_313371
Anti-mouse VCAM-1 PE (429)	BioLegend	Cat#105713; RRID:AB_1134166
Anti-mouse PDGFRβ Biotin (APB5)	BioLegend	Cat#136009; RRID:AB_2162325
Anti-mouse CD31 Alexa Fluor 647 (MEC13.3)	BioLegend	Cat#102516; RRID:AB_2161029
Anti-mouse CD31 Biotin (MEC13.3)	BioLegend	Cat#102504; RRID:AB_312911

Continued

REAGENT or RESOURCE	SOURCE	IDENTIFIER
Anti-mouse Sca-1 Alexa Fluor 647 (E13–161.7)	BioLegend	Cat#122518; RRID:AB_2143238
Anti-mouse VE-cadherin Alexa Fluor 647 (BV13)	BioLegend	Cat#138006; RRID:AB_10569114
Anti-mouse CXCR4 Biotin (L276F12)	BioLegend	Cat#146516; RRID:AB_2650787
IgG2b Isotype control Biotin (RTK4530)	BioLegend	Cat#400604; RRID:AB_326548
Anti-BrdU FITC (BU20A)	ThermoFisher Scientific	Cat#11-5071-42; RRID:AB_11042627
Anti-mouse/rat Ki-67 Alexa Fluor 488 (SolA15)	ThermoFisher Scientific	Cat#53-5698-82; RRID:AB_2802330
Anti-mouse I-A/I-E Biotin (M5/114.15.2)	BioLegend	Cat#107604; RRID:AB_313319
Anti-GFP (Polyclonal)	ThermoFisher Scientific	Cat#A-11122; RRID:AB_221569
Anti-Perilipin-1 (Polyclonal)	abcam	Cat#ab61682; RRID:AB_944751
Anti-mouse ALPL (Polyclonal)	R&D Systems	Cat#AF2910; RRID:AB_664062
Anti-mouse Ncr1 (Polyclonal)	R&D Systems	Cat#AF2225; RRID:AB_355192
Anti-rabbit IgG DyLight 488 (Polyclonal)	BioLegend	Cat#406404; RRID:AB_1575130
Anti-rabbit IgG DyLight 649 (Polyclonal)	BioLegend	Cat#406406; RRID:AB_1575135
Anti-goat IgG Alexa Fluor 647 (Polyclonal)	ThermoFisher Scientific	Cat#A-21447; RRID:AB_2535864
Chemicals, peptides, and recombinant proteins		
Sodium Azide	Fujifilm	Cat#199-11095
Paraformaldehyde	Fujifilm	Cat#168-23255
Sucrose	Fujifilm	Cat#196-00015
Neomycin sulfate	Sigma-Aldrich	Cat#1458009-200MG
Polymyxin B	Sigma-Aldrich	Cat#1547007-200MG
Hexane	Fujifilm	Cat#082-00426
Polyethylene glycol mono-*p*-isooctylphenyl ether (Triton X-100)	Nacalai Tesque	Cat#12967-45
5-Bromo-2′-deoxyuridine (BrdU)	Sigma-Aldrich	Cat#B5002
Bovine serum albumin (BSA)	Nacalai Tesque	Cat#01281-26
Collagenase D	Roche	Cat#11088882001
DNase I	Sigma-Aldrich	Cat#11284932001
Cellstain DAPI Solution	Dojindo	Cat#D523
Foxp3/Transcription Factor Staining Buffer Set	ThermoFisher Scientific	Cat#00-5523-00
BD Cytofix/Cytoperm Fixation/Permeabilization Kit	BD Biosciences	Cat#554714
Sepasol-RNA I Super G	Nacalai Tesque	Cat#09379-55
Citrate buffer saturated phenol	Nacalai Tesque	Cat#25968-64
Urea	Fujifilm	Cat#219-00175
N,N,N′,N′-tetrakis(2-hydroxypropyl) ethylenediamine	Tokyo Chemical Industry	Cat#T0781
2,2′,2′′-nitrilotriethanol	Tokyo Chemical Industry	Cat#S0377
Critical commercial assays		
MEBCYTO Apoptosis Kit	MBL	Cat#4700
EasySep Mouse NK Cell Isolation Kit	STEMCELL Technologies	Cat#19855
SMART-Seq v4 Ultra Low Input RNA Kit for Sequencing	Takara Bio	Cat#634890
Nextera XT DNA Library Prep kit	Illumina	Cat#FC-131-1024
Deposited data		
scRNA-seq of BM stromal cells	Baryawno et al.[34]	GEO: GSE128423

Continued

REAGENT or RESOURCE	SOURCE	IDENTIFIER
scRNA-seq of BM hematopoietic cells	The Tabula Muris Consortium[40]	https://figshare.com/projects/Tabula_Muris_Transcriptomic_characterization_of_20_organs_and_tissues_from_Mus_musculus_at_single_cell_resolution/27733
RNA-seq of immature NK cells and ILC1s from hematopoietic cell specific IL-15 cKO mice	This paper	GEO: GSE184586
RNA-seq of NK cells from Id2 KO mice	Delconte et al.[41]	GEO: GSE76466
RNA-seq of NK cells from Stat5 KO mice	Villarino et al.[44]	GEO: GSE100674
Experimental models: Cell lines		
B16-F10	ATCC	CRL-6475
Experimental models: Organisms/strains		
Mouse: C57BL/6	CLEA Japan or Japan SLC	MGI:2159769
Mouse: CD11c-Cre (Tg(Itgax-cre)1-1Reiz)	The Jackson Laboratory	MGI:3763248
Mouse: CX3CR1^{GFP} (Cx3cr1^{tm1Litt})	The Jackson Laboratory	MGI:2670351
Mouse: Lepr-Cre (Lepr$^{tm2(cre)Rck}$)	The Jackson Laboratory	MGI:3776158
Mouse: Rosa26^{YFP} (Gt(ROSA)26Sor$^{tm3(CAG-EYFP)Hze}$)	The Jackson Laboratory	MGI:3809521
Mouse: Rosa26^{tdTomato} (Gt(ROSA)26Sor$^{tm14(CAG-tdTomato)Hze}$)	The Jackson Laboratory	MGI:3809524
Mouse: Prx1-Cre (Tg(Prrx1-cre)1Cjt)	The Jackson Laboratory	MGI:2450929
Mouse: Il15^{CFP} (Il15$^{tm1.1Iku}$)	Previously generated in our lab[30]	MGI:5574316
Mouse: IL-15^{flox} (Il15^{tm2Iku})	Previously generated in our lab[53]	MGI:7263382
Mouse: Cxcr4^{flox} (Cxcr4^{tm2Tng})	Dr. Takashi Nagasawa (Osaka University)	MGI:3628644
Mouse: Cxcl12^{GFP} (Cxcl12^{tm2Tng})	Dr. Takashi Nagasawa (Osaka University)	MGI:3579534
Mouse: Tie2-Cre (Tg(Tek-cre)1Ywa)	Dr. Masashi Yanagisawa (University of Tsukuba)	MGI:2450311
Mouse: Ncr1-iCre (Tg(Ncr1-icre)265Sxl)	Dr. Veronika Sexl (University of Veterinary Medicine Vienna)	MGI:4941472
Mouse: Vav1-Cre (Tg(VAV1-cre)1Graf)	Dr. Thomas Graf (Center for Genomic Regulation)	MGI:3765313
Oligonucleotides		
qPCR Primer: Il15 5′-TGAGACCTGGCCACTTTCTC-3′	This paper	N/A
qPCR Primer: Il15 5′-TGGGCAGGATTAAGAGGAAC-3′	This paper	N/A
qPCR Primer: Hprt 5′-GTTGGATACAGGCCAGACTTTGTTG-3′	This paper	N/A
qPCR Primer: Hprt 5′-GATTCAACTTGCGCTCATCTTAGGC-3′	This paper	N/A
Software and algorithms		
Flowjo v10	BD Biosciences	https://www.flowjo.com/
Prism 8	GraphPad	https://www.graphpad.com/
R v3.6.3	The R Project for Statistical Computing	https://www.r-project.org/
Excel	Microsoft	https://www.microsoft.com/
LASX	Leica Microsystems	https://www.leica-microsystems.com/
Imaris 9	Oxford Instruments	https://imaris.oxinst.com/
Fiji	Schindelin et al.[54]	https://fiji.sc/

Continued

REAGENT or RESOURCE	SOURCE	IDENTIFIER
Trimmomatic v0.33	Bolger et al.[55]	http://www.usadellab.org/cms/?page=trimmomatic
Hisat2 v2.1.0	Kim et al.[56]	http://daehwankimlab.github.io/hisat2/
featureCount v1.6.5	Liao et al.[57]	https://subread.sourceforge.net/
edgeR v3.28.1	Robinson et al.[58]	https://bioconductor.org/packages/release/bioc/html/edgeR.html
Seurat v3.2.2	Stuart et al.[59]	https://satijalab.org/seurat/
ShinyGO v0.76	Ge et al.[60]	http://bioinformatics.sdstate.edu/go/
Other		
ReverTra Ace	Toyobo	Cat#TRT-101
TB Green Premix Ex Taq II	Takara Bio	Cat#RR820A
ProLong Glass Antifade Mountant	ThermoFisher Scientific	Cat#P36980
O.T.C compound	Sakura Finetek Japan	Cat#45833
Anti-mouse Ter-119 MicroBeads	Miltenyi Biotec	Cat#130-049-901
Anti-mouse CD45 MicroBeads	Miltenyi Biotec	Cat#130-052-301
MACS LD columns	Miltenyi Biotec	Cat#130-042-901
RNAClean XP	Beckman Coulter	Cat#A63987
Buffer LTR Qiagen	QIAGEN	Cat#79216

RESOURCE AVAILABILITY

Lead contact
Further information and requests for resources and reagents should be directed to and will be fulfilled by the lead contact, Koichi Ikuta (ikuta.koichi.6c@kyoto-u.ac.jp).

Materials availability
This study did not generate new unique reagents.

Data and code availability
- All next-generation sequencing data generated for this work have been deposited in the Gene Expression Omnibus (GEO) under accession number GEO: GSE184586. Accession numbers for other publicly available datasets reanalyzed in this paper are listed in the key resource table.
- The original code for quantifying NK cell localizations is available at GitHub on https://github.com/ShinyaABE0225/CellReports2023.
- Any additional information required to reanalyze the data reported in this paper is available from the lead contact upon request.

EXPERIMENTAL MODEL AND STUDY PARTICIPANT DETAILS

Mice
C57BL/6 (CD45.2) mice were obtained from CLEA Japan or Japan SLC. *CD11c-Cre*,[61] *CX3CR1*[GFP],[62] *Lepr-Cre*,[63] *Rosa26*[YFP],[64] *Rosa26*[tdTomato],[64] and *Prx1-Cre*[65] mice were also obtained from The Jackson Laboratories. *Il15*[CFP] mice have been reported previously.[30] *IL-15*[flox] mice were generated in our laboratory.[53] *Cxcr4*[flox][66] and *Cxcl12*[GFP][67] mice were provided by Dr. Takashi Nagasawa (Osaka University). *Tie2-Cre* mice were kindly provided by Dr. Masashi Yanagisawa (University of Tsukuba) and locally supplied by Dr. Atsuko Sehara-Fujiwara (Kyoto University).[68] *Ncr1-iCre*[69] mice were provided by Dr. Veronika Sexl (University of Veterinary Medicine Vienna). *Vav1-Cre*[70] mice were kindly provided by Dr. Thomas Graf (Center for Genomic Regulation) and locally supplied by Dr. Manabu Sugai (University of Fukui). All mice were maintained under specific pathogen-free conditions at the Experimental Research Center for Infectious Diseases, the Institute for Life and Medical Sciences, Kyoto University, and used according to the protocol approved by the Animal Experimentation Committee of the Institute. All procedures were performed under anesthesia to minimize animal suffering. Each pair of control and mutant mice of the same sex from the same litter was analyzed simultaneously, and the data from multiple pairs of mixed-sex mice from multiple litters were pooled.

METHOD DETAILS

Cell isolation

BM cells were collected from the tibia and femur. Spleen cells were prepared by mechanically crushing the organs with a cell strainer. The cell density of PB was measured using an automatic blood cell counter (Celltac α MEK6450, Nihon Kohden Corp.). BM, spleen, and blood cells were treated with ACK buffer to lyse red blood cells. To prepare BM stromal cells, the BM plug was digested in RPMI-1640 medium containing 0.1% collagenase D (Roche) and 0.01% DNase I (Sigma-Aldrich) for 40 min at 37°C with shaking. Digested BM cells were incubated with magnetic beads conjugated to anti-CD45 and Ter119 antibodies, and hematopoietic cells were depleted using MACS LD columns (Miltenyi Biotec).

Flow cytometry and cell sorting

Cells were stained with antibodies for 20 min at 4°C in PBS containing 0.05% NaN_3 and 0.1% bovine serum albumin (BSA). Fluorescent dye- or biotin-conjugated antibodies against the following proteins were purchased from BioLegend, Invitrogen, or TONBO Biosciences: CD3ϵ (145-2C11), NK1.1 (PK136), CD127 (A7R34), CD49a (Ha31/8), CD49b (DX5), CD27 (LG.7F9), CD11b (M1/70), NKp46 (29A1.4), Eomes (Dan11mag), TCRβ (H57-597), CD4 (RM4.5), CD8α (53–6.7), CD44 (IM7), CD45R/B220 (RA3-6B2), CD19 (6D5), CD45 (30-F11), CD45.1 (A20), CD45.2 (104), CD122 (TM-beta1), 2B4 (eBio244F4), Flt3 (A2F10), PD-1 (29F.1A12), CD25 (PC61), CD11c (N418), FcϵR1 (MAR-1), Ly-6D (49-H4), Ter-119 (Ter-119), CD115 (AFS98), Gr-1 (RB6-8C5), VCAM-1 (429), PDGFRβ (APB5), CD31 (MEC13.3), Sca-1 (E13–161.7), CXCR4 (L276F12) and IgG2b isotype (RTK4530). CD1d tetramer was kindly provided by the NIH Tetramer Core Facility at Emory University. Biotinylated monoclonal antibodies were detected with PE- or Brilliant Violet 421-conjugated streptavidin (Invitrogen). The lineage marker cocktail contains the following antibodies: CD3, CD4, CD8α, CD11b, CD11c, Gr-1, Ter119, CD19, and NK1.1 for ILCP staining, and Ly-6D is added for rNKP staining. For the intracellular staining of Eomes, cells were stained for surface antigens, fixed, permeabilized, and stained with antibodies using the Foxp3 Staining Buffer Set (Invitrogen). For the intracellular staining of tdTomato-positive cells from Rosa26-tdTomato reporter mice, the cells were fixed with 3% formaldehyde, permeabilized, and stained with antibodies using the Foxp3 Staining Buffer Set. Annexin V staining was performed using the MEBCYTO Apoptosis Kit (MBL life science) according to the manufacturer's instructions. Stained cells were measured on an LSRFortessa flow cytometer (BD Biosciences), and fcs files were analyzed using FlowJo software (BD Biosciences). For CAR cell sorting, stained samples were aliquoted into PBS containing 5% FBS using a FACS Aria III cell sorter (BD Biosciences) equipped with a 100 μm nozzle. CAR cells were gated as CD45$^-$Ter119$^-$CD31$^-$VCAM-1$^+$PDGFRβ^+. CAR cell purity was >95%, as determined by FCM. In the figures, values in quadrants, gated areas, and interval gates indicate percentages in each population.

BrdU incorporation

Mice were injected intraperitoneally with 5 mg BrdU (Sigma-Aldrich) diluted in PBS 3 times at 4-h intervals. BM was harvested 12 h after the last dose. Surface-stained cells were fixed and permeabilized with Cytofix/Cytoperm (BD Biosciences) and treated with DNase I for 1 h at 37°C. Cells were stained with FITC-conjugated anti-BrdU antibody (BA20A, Invitrogen) for 30 min at room temperature and analyzed on an LSRFortessa flow cytometer (BD Biosciences).

Cell culture

CD19$^+$ B cells, CD19$^-$CD115$^+$Gr-1$^-$ monocytes, CD19$^-$CD115$^-$Gr-1$^+$ neutrophils, and CD19$^-$CD115$^-$Gr-1$^-$c-kit$^+$ hematopoietic progenitors were sorted on a FACS Aria III cell sorter for NK cell co-culture (BD Biosciences). Splenic NK cells from CD45.1 WT mice were enriched using the EasySep mouse NK cell isolation kit (STEMCELL Technologies), and NK1.1$^+$CD3ϵ^- NK cells were sorted on the FACS Aria III cell sorter. A total of 2×10^5 B or myeloid cells and 1.5×10^4 NK cells were co-cultured in RPMI 1640 medium containing 10% FBS in a 96-well U-bottom plate. After 24 h, PI$^-$ CD45.1$^+$ cells were counted using an LSRFortessa flow cytometer.

Bone marrow transplantation

To generate BM chimeric mice, 8-week-old IL-15-flox and Tie2-Cre; IL-15-flox mice were irradiated with two doses of 4.5 Gy separated by 3 h. Irradiated mice were reconstituted with 2×10^5 BM cells from CD45.1 mice by intravenous injection. Recipient mice were evaluated 5 weeks after the transplantation. Mice were fed with acidic water (pH 2.5) for 2 days before irradiation and water containing 1 g/L neomycin sulfate (Sigma-Aldrich) and 1 MU/L polymyxin B sulfate (Sigma-Aldrich) for 2 weeks after the irradiation to improve the viability of the irradiated mice.

Real-time RT-qPCR

Total RNA was extracted with Sepasol-RNA I Super G (Nacalai Tesque) and treated with citrate buffer-saturated phenol (Nacalai Tesque). Genomic DNA was digested with DNase I, and RNA was reverse transcribed using ReverTra Ace (TOYOBO) and random primers (Thermo Fisher Scientific). cDNA was amplified in duplicate on a StepOnePlus Real-Time PCR System (Thermo Fisher Scientific) using TB Green Premix Ex Taq II (Takara) and ROX reference dye (Takara). After amplification, a melting curve analysis was performed to verify the specificity of the reaction. Transcript levels were normalized to hypoxanthine-guanine phosphoribosyltransferase (HPRT)

mRNA. Primer sequences were as follows: *Il15*, 5′-TGAGACCTGGCCACTTTCTC-3′ and 5′-TGGGCAGGATTAAGAGGAAC-3′; and *Hprt*, 5′-GTTGGATACAGGCCAGACTTTGTTG-3′ and 5′-GATTCAACTTGCGCTCATCTTAGGC-3′.

Immunofluorescence analysis

Freshly harvested tissues were fixed in 4% paraformaldehyde (PFA) at 4°C for 7 h and replaced with a solution of 10%, 20%, and 30% sucrose in PBS at 4°C for 3 days. Tissues were embedded in O.T.C. compound (Sakura Finetek Japan) and frozen in cooled hexane. Sections 8-μm thick were prepared using the Kawamoto film method and a Leica cryostat.[71] Sections were blocked with PBS containing 10% BSA and 0.2% Triton X-100 (Nacalai Tesque) for 1 h at room temperature before staining. Primary antibodies were applied to the slides for 2 h at room temperature, followed by secondary antibody incubation for 30 min at room temperature. The following primary antibodies were used: anti-GFP (Invitrogen), anti-S100 (Dako), anti-perilipin (Abcam), anti-ALPL, and anti-Ncr1 (R&D Systems). Alexa Fluor 488-anti-Ki-67 (SolA15), Alexa Fluor 647-anti-VE-cadherin (BV13), Alexa Fluor 647-anti-Sca-1 (E13–161.7), and Alexa Fluor 647-anti-CD31 (390), biotin-anti-I-A/I-E (M5/114.15.2) were also used as the primary antibodies and were purchased from Biolegend and Invitrogen. DyLight 488-anti-rabbit IgG (BioLegend), DyLight 649-anti-rabbit IgG (BioLegend), Alexa Fluor 647-anti-goat IgG (Invitrogen), and BV421-streptavidin (Biolegend) were used as the secondary antibodies. For nuclear staining, sections were treated with 4′,6-diamidino-2-phenylindole (DAPI). Stained sections were mounted with Prolong Glass (Thermo Fisher Scientific).

Images were acquired on a Leica SP8 confocal microscope equipped with HC PL APO CS2 20×/0.75 IMM or HC PL APO CS2 40×/1.30 OIL objectives and analyzed using LASX (Leica) and the Fiji build of ImageJ (NIH).[54] For the *in situ* mapping analysis, the images acquired by the tile scans were merged, and a maximum intensity projection in LASX assembled their z stack images of 10 μm depth at 1 μm intervals. Segmentation of Ncr1-tdTomato+ NK cells was performed by Fiji with a threshold function and registered as a region of interest (ROI). Each ROI was checked individually, and if multiple cells were registered as one region, they were re-registered while checking the z stack images. The z stack images confirmed the Ki-67 and CD11b expression of each ROI, and the attributes of NK cells in each ROI were registered. The blood vessels were binarized and highlighted by a morphology filter, and the remaining fine noise was manually removed. Ki-67+ random cells were segmented by a threshold function and randomly selected from all registered ROIs. The same number of random and NK cells were selected in each image using the RANDBETWEEN function in Excel (Microsoft). Center of mass coordinates were exported from the ROIs of NK cells or random cells. To obtain distances to neighboring cells, the distances to all center-of-mass coordinates were calculated using R (version 3.6.3), from which the distances to the first to sixth nearest neighbors were extracted. For the distance to the blood vessel, an edge extraction was performed on the image after applying a morphology filter. The distance was calculated for all pixels on the edge of the vasculature in the same way as above, and the nearest distance was extracted. The clustered region was defined as an area with an NK cell density greater than 5 cells/100 μm^2 including more than 20 cells in a two-dimensional field. Additional information and the R code are available upon request.

Tissue clearing and deep imaging of bone marrow

To visualize blood vessels, mice were injected intravenously with 10 μg Alexa Fluor 647-conjugated anti-VE-cadherin and anti-CD31 antibodies (Biolegend) and sacrificed 5 min later. Tibia, femur, and spleen were fixed in 4% PFA at 4°C for 7 h and then replaced with 10%, 20%, and 30% sucrose. Tissues were embedded in O.T.C. compound and sectioned at 500 μm thickness using a Leica Cryostat. For whole-mount imaging of BM and spleen, the CUBIC tissue-clearing method was used.[32] Trimmed tissues were washed with PBS for 1 h at room temperature. The tissues were then immersed in 50% diluted Sca/eCUBIC-1 (reagent 1) at 37°C for 4 h and in plain Sca/eCUBIC-1 (reagent 1) at 37°C overnight. Tissues were washed with PBS for 3 h and immersed in 50% diluted Sca/eCUBIC-2 (reagent 2) for 4 h and plain Sca/eCUBIC-2 (reagent 2) at 37°C overnight. Sca/eCUBIC-1 (reagent 1) was prepared as a mixture of 25 wt% urea, 25 wt% *N,N,N′,N′*-tetrakis(2-hydroxypropyl)ethylenediamine (Tokyo Chemical Industry), and 15 wt% polyethylene glycol mono-*p*-isooctylphenyl ether/Triton X-100. Sca/eCUBIC-2 (reagent 2) was prepared as a mixture of 50 wt% sucrose, 25 wt% urea, 10 wt% 2,2′,2″-nitrilotriethanol (Wako Pure Chemical Industries), and 0.1% (v/v) Triton X-100. Images of transparent sections were captured on a Leica SP8 confocal microscope equipped with HC PL APO CS2 20×/0.75 IMM objectives.

Images were analyzed using LASX or Imaris software (Bitplane Scientific). For the spatial analysis of NK cells, tile-scan images were merged by LASX, and merged images were reconstructed in three dimensions by Imaris. NK cells were replaced by spheres using the spot function of Imaris, where the diameter of the cell was set to 8 μm. The 3D coordinates of the NK cell spots were then exported. To make the analysis consistent, the volume of one marrow was set to 800 μm × 2,400 μm × 100 μm. Random cell coordinates were assigned using the RANDBETWEEN function in Excel, and random cells were placed in the same space at the same density as the NK cell spots. The reciprocal distance of all NK or random cells was calculated based on the coordinate values.

RNA preparation and next-generation sequencing

Flow-sorted NK cells were immediately lysed with buffer LTR (Qiagen) and purified with RNAClean XP (Beckman Coulter). Double-stranded cDNA was synthesized using the SMART-Seq v4 Ultra Low Input RNA Kit for Sequencing (Takara), and sequencing libraries were constructed using the Nextera XT DNA Library Preparation Kit (Illumina) according to the manufacturer's instructions. Libraries were sequenced using 150 bp paired-end reads on an Illumina HiSeq X Ten sequencer (Illumina). Raw sequenced reads were filtered using Trimmomatic (version 0.33) to exclude low quality sequences.[55] The filtered sequences were aligned to the mouse reference

genome (mm10) using Hisat2 (version 2.1.0),[56] and the aligned reads were used for the transcript quantification by using feature-Count (version 1.6.5).[57] To identify genes that could be reliably used to analyze each cell population, we first filtered out genes with low counts using the filterByExpr function (min.count = 1) of edgeR (version 3.28.1).[58] 33,293 and 33,637 genes remained after filtering for iNK2 cells and iILC1s, respectively. DEGs were identified by the exact test of edgeR (FDR< 0.1). Enrichment analysis of the KEGG pathway and TFact database was performed using ShinyGO v0.61.[60]

scRNA-seq analysis
BM stromal cell data were obtained from the GSE dataset accession no. GSE128423,[34] and BM hematopoietic cell data were extracted from figshare (https://figshare.com/projects/Tabula_Muris_Transcriptomic_characterization_of_20_organs_and_tissues_from_Mus_musculus_at_single_cell_resolution/27733).[40] Clustering and gene expression analyses were performed using the Seurat R package (version 3.2.2).[59] Genes expressed in fewer than 3 cells and cells with no more than 200 detected genes were filtered out. We also removed cells with more than 5% mitochondrial genes for the stromal cell dataset. We applied library size normalization to each cell using the NormalizeData function with default settings. Highly variable genes were screened for the downstream analysis using the FindVariableFeatures function. Principal component analysis (PCA) was performed on the 2,000 variable genes using the RunPCA function. Based on the ElbowPlot results, we decided to use 30 and 16 principal components to cluster the stromal cell and hematopoietic cell datasets, respectively. The resolution parameters of the FindCluster function were set to 0.1 for both datasets. For the stromal cell dataset, FindAllMarkers (only.pos = TRUE, min.pct = 0.25, logfc.threshold = 0.25) was used to identify the clusters of hematopoietic cells (CD45$^+$) to be removed. The remaining cells were then recalculated using the FindNeighbors and FindCluster functions. Cells within the clusters were visualized on a UMAP plot using RunUMAP, and FeaturePlot was used to visualize individual gene expressions on a UMAP plot. The cell type labeling of each cluster is based on the result of FindAllMarkers and FeaturePlot. Any additional information needed to reanalyze the data reported in this paper is available upon request from the lead contact.

QUANTIFICATION AND STATISTICAL ANALYSIS

All data are presented as individual values with means, and error bars indicate ±SEM. Data were tested using either unpaired two-tailed Student's t-test (normal distribution) or ANOVA (one-way or two-way as appropriate). Asterisks in all figures indicate the following: $*p < 0.05$, $**p < 0.01$, and $***p < 0.001$. Statistical analyses were performed using Prism8 software (GraphPad).